UNIVERSIDADE DE LISBOA
FACULDADE DE CIENCIAS
DEPARTAMENTO DE FÍSICA


# The Feasibility of SmART (Small Animal Radiation Therapy) Platform for Delivering Complex Dose Distributions

Joana Batista Verde

Mestrado Integrado em Engenharia Biomédica e Biofísica
Perfil em Radiações em Diagnóstico e Terapia

Dissertação orientada por:
Professor Frank Verhaegen e Professor Luís Peralta

[2016]

# ACKNOWLEDGEMENTS

Hereby, I would like to address my gratitude to all the people who helped me to perform my master´s project, write this thesis, and who made the last year at MAASTRO Clinic such a great time. First and foremost, I would like to express my gratitude to both my external supervisors. My sincere thanks to Dr. Frank Verhaegen, head of physics research at MAASTRO Clinic, for giving me the opportunity to be a part of his exciting research division, by engaging me in new ideas and demanding a high quality of work. I am extremely thankful to Stefan van Hoof for being always there to listen and give advices, for his patience, motivation, enthusiasm, and immense knowledge. I am also grateful to him for the long discussions that helped me sort out the technical details of my work and for the encouragement to use the correct grammar and consistent notation in my writings.

I wish to thank Professor Luís Peralta for being my internal supervisor and for all the support through this learning process.

Special thanks to Isabel de Almeida for the laughing moments together and all the funny stories. Another special thanks to Lotte Scyns for all her useful advice, her help with measurements and also for her enthusiastic support to Cristiano Ronaldo and to the National Portuguese team. My profound gratitude to the whole research group of MAASRO Clinic with whom I had the privilege to work and who I have not already mentioned: Matilde Costa, Mark Podesta, Gabriel Fonseca, Murillo, Ruben, Janita, Sara, Brent, Timo, Jurgen, Ivonka, Shane, Shaun, Aniek, Guacomo, Cecile and Ana Vaniqui. They provided a friendly and cooperative atmosphere at work and entertainment during lunch and coffee breaks.

My deepest sincere thanks to Mariana Brás for all the support during this journey, as well as for her patience, help and laughs who made my days easier.

I am very grateful to the Professors of the Institute of Biophysics and Biomedical Engineering for all the dedication, time, encouragement and knowledge that they shared with me during the last five years.

To my friends and roommates, thank you for listening, offering me advice, and supporting me through this entire process, thank you for the phone calls, e-mails, texts, editing advice, and especially for being there whenever I needed.

Most importantly, none of this would have been possible without the love and patience of my family. My immediate family to whom this dissertation is dedicated to, has been a constant source of love, concern, support and strength all these years. Thus, I would like to express my heart-felt gratitude to them. They supported and encouraged me throughout this endeavor and, therefore I warmly appreciate their unconditional generosity and understanding.

# RESUMO

O cancro é atualmente a segunda principal causa de morte na Europa, encontrando-se apenas atrás das doenças cardiovasculares. O cancro surge quando as células normais se começam a transformar em células cancerígenas. Isto é, quando as células adquirem a capacidade de se multiplicarem e invadirem os tecidos e outros órgãos. Na União Europeia, uma previsão realizada pela International Agency for Research on Cancer (IARC), e tendo como base apenas o envelhecimento da população, aponta para um aumento de novos casos de cancro na ordem dos 24 milhões até 2035.

O tratamento eficaz do cancro deve dirigir-se não apenas ao tumor principal, mas também aos tumores que possam aparecer, por propagação. No combate contra o cancro existem atualmente diferentes tratamentos como a cirurgia, a radioterapia, a quimioterapia ou uma combinação destas diferentes técnicas. Hoje em dia cerca de 4 em cada 10 doentes oncológicos (40%) em alguma etapa do tratamento da sua doença, são submetidos a tratamentos de radioterapia. Esta é uma modalidade terapêutica utilizada sobretudo no tratamento de doenças oncológicas, que usa radiação ionizante como os raios X para lesar ou destruir as células dos tumores malignos. Consoante a localização da fonte de radiação em relação ao corpo do paciente podem existir duas formas da radioterapia: radioterapia interna, na qual a radiação tem origem a partir de uma fonte que é colocada no interior do organismo e radioterapia externa, na qual a fonte de radiação se encontra a uma certa distância do paciente, sendo gerada na sua maioria das vezes por aparelho chamado acelerador linear.

Os tratamentos de radioterapia concentram-se na destruição das células tumorais, ao mesmo tempo que se concentram na necessidade de minimizar ao máximo a exposição dos tecidos sãos adjacentes à radiação. De maneira a ter tratamentos onde a radiação se restrinja cada vez mais ao tumor enquanto há uma minimização da exposição dos tecidos saudáveis adjacentes, novas técnicas de radioterapia têm aparecido ao longo das últimas décadas como são exemplo a radioterapia tridimensional conformal (3D-CRT), a radioterapia de intensidade modulada (IMRT), a radioterapia guiada por imagem (IGRT) entre outras.

Uma validação experimental destas técnicas é crucial antes da sua implementação em ambiente clínico. Uma vez que é difícil validar novas técnicas com base em dados humanos, devido às preocupações práticas e éticas, a validação experimental baseada em pequenos animais apareceu como uma abordagem alternativa e mais rápida, o que faz da radioterapia em pequenos animais um campo de pesquisa ativo atualmente, provado pelo forte investimento e procura de plataformas de radioterapia para pequenos animais por parte de diferentes institutos. Este tipo de plataformas de radioterapia para pequenos animais tem também o valor acrescentado de permitir estudar e avaliar a eficácia de diferentes terapias anticancerígenas através do estudo de mecanismos de resposta das doenças cancerígenas. Estas plataformas são também importante para estudar a resposta dos tecidos cancerígenos e dos tecidos normais à exposição de radiação, assim como na avaliação da segurança de novos medicamentos anticancerígenos.

Apesar do grande desenvolvimento e consequente aparecimento de diferentes plataformas de radioterapia para pequenos animais existe um fator limitante comum a todas elas. Atualmente neste tipo de plataformas os tratamentos baseiam-se principalmente em técnicas de irradiação primitivas. Nestas técnicas os tratamentos são baseados em um ou dois feixes estáticos de

radiação muitas vezes envolvendo uma irradiação total ou parcial do corpo, o que faz destes tratamentos uma abordagem nada representativa do que realmente acontece em ambiente clínico. Para que hajam tratamentos mais representativos e com configurações mais semelhantes ao que acontece em ambiente clínico, planos de tratamento mais complexos onde seja possível entregar distribuições de dose mais complexas e heterogéneas são necessários. Desta forma, o objetivo deste estudo é investigar a capacidade da plataforma de radioterapia para pequenos animais, XRAD-225Cx, de entregar distribuições de dose mais complexas através do movimento da mesa de tratamento e da *gantry* durante o tratamento. Adicionalmente , é também investigado a necessidade de graus de liberdade adicionais em radioterapia em pequeno animais através de simulações de tratamentos com diferentes configurações de feixes de radiação.

A plataforma de radioterapia para pequenos animais utilizada neste estudo foi a plataforma *Precision X-Ray XRAD-225Cx* que se encontra instalada na MAASTRO Clinic (Maastricht, Holanda). No que diz respeito às simulações dos tratamentos, estas foram simuladas com recurso ao software, SmART-Plan, um sistema de plano de tratamento desenvolvido no departamento de radioterapia da MAASTRO Clinic. Este é um software desenvolvido em MATLAB baseado num algoritmo de Monte-Carlo.

Distribuições de dose mais complexas podem ser conseguidas através do movimento simultâneo de mesa de radioterapia e da *gantry* durante o tratamento. A viabilidade desta técnica foi investigada através da utilização de planos de tratamento baseados em pontos de controlo, os quais são designados de protocolos. Um protocolo é um documento de texto estruturado onde estão descritas de uma forma sequencial as diferentes etapas e variáveis de um tratamento Um protocolo é dividido num número de feixes e cada feixe é dividido em pontos de controlo. Um ponto de controlo específica o comportamento da plataforma num momento específico de tempo, isto é, especifica a maneira como é que o tratamento é entregue. Em cada ponto de controlo pode ser especificado o posicionamento e movimento da mesa de radiação e da *gantry*, o ângulo e o sentido de rotação da *gantry*, a energia do feixe, o período de irradiação e a dose entregue em cada ponto de controlo.

Nesta tese o posicionamento da mesa de tratamento foi verificado e avaliado através de um sensor de ultra-som. De maneira a avaliar o movimento da mesa de tratamento, protocolos com diferentes números de pontos de controlo foram testados. O movimento da mesa de tratamento foi avaliado ao longo das 3 direções do movimento, longitudinal, lateral e vertical. Depois de uma correta avaliação do movimento da mesa de tratamento, os tratamentos baseados em pontos de controlo foram avaliados em termos de distribuição de dose através de filmes radiocrómicos, os quais foram posteriormente comparados com simulações.

A quantidade de número de graus de liberdade pode ser aumentada através da rotação da mesa de tratamento e da *gantry*, o que permite a entrega de feixes de radiação a partir de qualquer ângulo. De maneira a perceber se a entrega de feixes a partir de diferentes direções pode melhorar as distribuições de dose e consequentemente os tratamentos aplicados, foram considerados 2 casos diferentes. Em ambos os casos as simulações foram baseadas em imagens de tomografia computorizada de feixe cónico. O primeiro caso dizia respeito a um rato com um glioblastoma multiforme e o segundo caso era baseado num rato com um tumor no pulmão. Os planos de tratamento foram avaliados com base em histogramas de volume-dose e nas respetivas métricas.

Nesta tese foram entregues pela primeira vez distribuições de dose complexas através de tratamentos baseados no movimento da mesa de tratamento e da *gantry* com recurso a pontos de controlo. Os resultados indicam um posicionamento preciso, confiável e reprodutível da mesa de tratamento durante todo o tratamento. Foi também provado que o irradiador consegue entregar tratamentos com um elevado número de pontos de controlo sem dificuldades. O estudo relativo às distribuições de dose mostrou uma elevada concordância entre os resultados obtidos com os filmes radiocrómicos e as respetivas simulações.

Relativamente aos resultados acerca da necessidade de graus de liberdade em radioterapia com pequenos animais no caso do glioblastoma, estes indicam que tratamentos com feixes entregues de diferentes ângulos não melhoram a qualidade do tratamento em comparação com os tratamentos padrão feitos hoje em dia em radioterapia com pequenos animais. Em contrapartida, as simulações de diferentes planos de tratamento do caso referente ao tumor no pulmão mostraram que gaus de liberdade adicionais podem melhorar o tratamento desde que sejam utilizadas as configurações geométricas do feixe mais corretas.

# ABSTRACT

The aim of radiation therapy is to deliver a very high dose of radiation to a tumor, while trying to spare the surrounding normal tissues. Due to the need of dose distributions improvement, over the past two decades radiotherapy underwent through a series of developments where new complex radiotherapy techniques appeared. Meanwhile, these techniques are currently implemented in clinical practice without enough experimental validation. To face this problem, small animal irradiators can be a new platform for testing new treatment possibilities. There is a limitation in current small animal experiments where the treatments are mostly based on primitive irradiation techniques that are not representative of what really happens in clinical practice. To better mimic pre-clinical treatments to the ones used in clinical practice, more complex treatment plans with the possibility of delivering more complex and heterogeneous dose distributions are needed. In this way, the purpose of this study is to investigate the capability of the XRAD-225Cx microirradiator to deliver complex dose distributions through stage and gantry movements along with the need of additional degrees of freedom in pre-clinical treatments.

Treatment plans were delivered using the pre-clinical radiotherapy platform Precision X-Ray XRAD-225Cx installed at MAASTRO Clinic (Maastricht, Netherlands) of which the absolute stage positioning was verified using an ultra sound sensor. More complex dose distributions can be achieved by using simultaneous table and gantry movement during irradiation and the feasibility of this technique was investigated through the use of control point (CP) based treatment plans consisting of high numbers of control points. The need for additional degrees of freedom in small animal radiotherapy was evaluated using cone-beam CT scans of 2 tumor bearing mice, a glioblastoma multiform (GBM) case and a lung tumor case. The tumors and the organs at risk (OAR) were delineated for both cases to simulate and evaluate different treatment plans in which different degrees of freedom were taken into account. To simulate all the treatments, a research version of the Monte Carlo based treatment planning system, SmART-Plan was used.

The results indicate an accurate, reliable and reproducible stage positioning during treatment delivery. The XRAD-225Cx proved to be able to deliver treatment plans with high number of control points and also proved to be able of delivering complex dose distributions through stage and gantry movement. Results from different GBM treatment plans indicate that treatments with additional degrees of freedom do not considerably improve treatment plan quality in comparison with standard treatments done nowadays in preclinal practice. In contrast, the simulations of lung tumor treatment plans showed that is possible that additional degrees of freedom with correct geometric beam configurations may improve the treatment.

**keywords:** small animal radiotherapy**,** XRAD-SmART, Smart-Plan, dose distribution, degrees of freedom

## LIST OF FIGURES

## LIST OF TABLES

## LIST OF ABREVIATIONS

| | |
|---|---|
| 2D | Two dimensional |
| 3D | Three dimensional |
| ADC | Analog to Digital Convertor |
| CBCT | Cone beam computed tomography |
| COV | Coefficient of variance |
| CP | Control point |
| CRT | Conformal radiotherapy |
| CT | Computed tomography |
| dof | Degrees of freedom |
| DPI | Dots per inch |
| DVH | Dose volume histogram |
| Gy | Gray |
| HU | Hounsfield units |
| IARC | International agency for research on cancer |
| IGRT | Image-guided radiation therapy |
| IMRT | Intensity modulated radiation treatment |
| kV | Kilo volt |
| kVp | Kilo volt peak |
| kW | Kilo watt |
| mA | Milliampere |
| MRI | Magnetic resonance imaging |
| PET | Positron emission tomography |
| SAIGRT | Small animal image-guided radiation therapy |
| SARRP | Small animal radiation research platform |
| SDD | Source to detector distance |
| SID | Source to isocenter distance |
| SmART | Small animal radiation therapy |
| std | Standard deviation |
| TPS | Treatment planning system |
| US | Ultra sound |
| WHO | World health organization |

# TABLE OF CONTENTS

# 1. INTRODUCTION

## 1.1. General introduction and motivation

Cancer is the main cause of death and morbidity in Europe after cardiovascular diseases (WHO, 2015). According to the International Agency for Research on Cancer (IARC), in 2012, 14.1 million new cases of cancer appeared worldwide causing 8.2 million cancer related deaths (Stewart & Wild, 2014). The number of new cases of cancer is expected to increase to 24 million by 2035 (WCRF International). Generally, cancer occurs when the normal cells in the body start growing in an uncontrolled way. There are many different types of cancer and they are typically named for the organ or the cell where the cancer begins. Some causes of cancer can be prevented but others, such as family history or aging cannot. In this way, early detection and better treatments are the best way to improve the cure.

Radiotherapy plays an important role in cancer treatment since the discovery of X-Rays by Röntgen in 1895. Presently, almost 40% of all people with cancer have radiotherapy included on their treatment plan (CRUK, 2015). In radiotherapy, ionizing radiation is targeted to cancerous tissue in order to control tumor growth by causing cell death, which is possible due to the use of high energy beams of different types of energy like photons or charged particles. Ionizing radiation works by damaging the DNA of cancer cells leading to cellular death. Nearby healthy tissues also suffer temporary cell damage from radiation, but these cells are usually able to repair the DNA damage and continue growing normally (NIH, 2010). The treatment success is strongly correlated with the damage on cancer cells and the sparing of the healthy surrounding tissues. The amount of ionizing radiation delivered during a treatment is expressed as absorbed dose, measured in units of Gray (Gy), i.e. energy deposited per unit of mass ($J.Kg^{-1}$). Radiotherapy can be performed by using external or internal radiation therapy. The most common type of radiation treatment is external radiotherapy and involves the delivery of radiation by a source that is located outside the patient body. In this case, the radiation is delivered by a linear accelerator which focuses high-energy radiation beams onto the area that requires treatment. In internal radiotherapy, also called brachytherapy, the radiation source is placed inside/near the tumor. Currently, radiotherapy can be used alone or in combination with chemotherapy. Furthermore, it can also be used before surgery to shrink a tumor, or after surgery to destroy tumor cells that may be left.

Great technological advances have been taking place in radiation therapy over the couple last decades where new focused radiation techniques appeared, as 3-dimensional conformal radiotherapy (3D-CRT), intensity modulated radiation treatment (IMRT), image-guided radiation therapy (IGRT), stereotactic radiosurgery and dose painting. These techniques use advanced medical imaging techniques for targeting, use local beam intensity modulation and focused beams delivered from many different angles allowing the spare of the tumor adjacent healthy tissues.

An increasing effort to improve the different radiotherapy techniques and to develop new ones in order to improve the efficiency of the radiation therapy treatments is evident. With the emergence of new techniques, radiobiological experiments and experimental validation are crucial before the implementation of these techniques in a clinical environment. Once it is really difficult to validate new techniques based on human trials due to practical and ethical concerns associated with human experiments, animal experiments appear as an essential approach in cancer research. This makes Small Animal Radiation Therapy an upcoming research field. More and more researchers and institutions recognize the importance of small animal radiation

therapy, which is shown by the acquisition of this kind of platforms from more than 60 radiotherapy centers.

The concept of radiotherapy, where cells are damaged by radiation, for small animals is equivalent to the human concept, whereby the radiation device for small animal radiotherapy is similar but of smaller dimensions. However, downscaling radiation therapy from a clinical setting to a smaller pre-clinical setting is not as simple as a geometric adjustment. For example in clinical practice, the treatment planning and the irradiation of the patient can take days or weeks. Though, in pre-clinical treatments the treatment process is performed while the animal is under anesthesia and the entire treatment has to be performed within 20 to 90 minutes in total (Figure 1). Another major difference between clinical practice and small animal radiation treatments is the different size of the body of humans and small animals, as rats or mice, which leads to the need of radiation beams in the mm scale with a sub-millimeter precision.

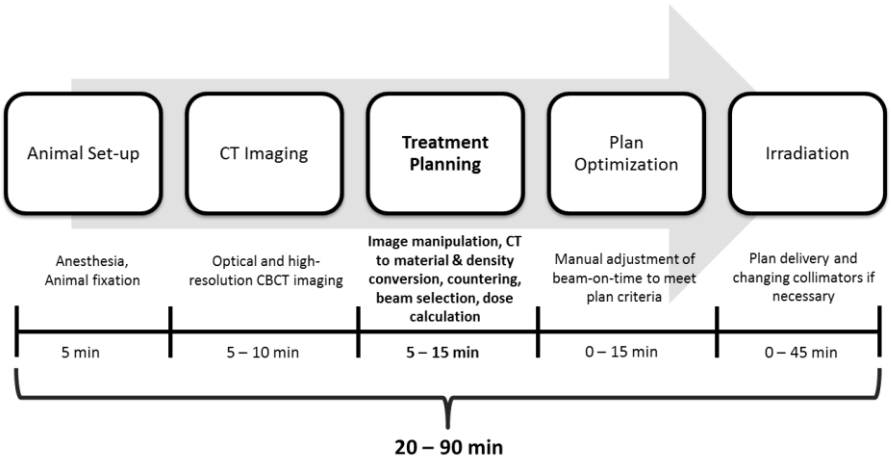


**Figure 1** – Schematic overview of the different phases in precision small animal radiotherapy and the duration of each phase. Adapted from (Balvert, 2015).

The recent development and commercialization of new small animal image-guided radiotherapy devices has made small animal radiotherapy experiments possible. These devices offer precise irradiation with Cone Beam Computed Tomography (CBCT) guidance and bioluminescence tomography for improved targeting. Several groups have recently started improving some existing systems and developing new research systems that allows precise irradiation of the tumors in small animals (Verhaegen et al., 2011).

These new small animal irradiation platforms also offer treatment planning systems (TPS) with 3D dose distribution and dose volume histograms (DVH) of the structures of interest. DVHs are usually used to evaluate the treatment plan. A DVH is a histogram relating the radiation dose delivered to a tissue volume. Treatment plans are created based on 3D images produced using Computed Tomography (CT) or Magnetic Resonance (MR) images. Assimilating the vast amount of information in a 3D radiation dose array is very difficult and DVH condenses this vast information into easily interpretable 2D graphs. There are two types of DVHs commonly used: differential and cumulative DVHs. The most common one is the cumulative dose-volume histogram (cDVH). This DVH displays the percentage number of voxels in a volume which receives at least a dose D. The cumulative DVH always begins at 100% (100% of the structures receive at least 0 dose). Thus for an ideal treatment plan, the DVH of the target volumes will have a rectangular, step-down function appearance and the DVH of the organs at risk will drop

immediately to zero (Figure 2). A drawback of the DVH methodology is that it offers no spatial information.

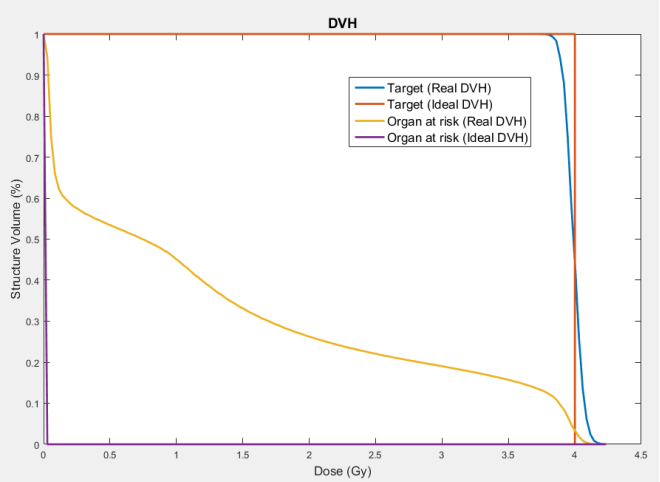


**Figure 2 -** Cumulative Dose Volume Histogram representation for two different structures, target (e.g. tumor) and organ at risk, with a prescribed dose of 4Gy. The ideal and the real DVH are also represented for these two structures.

## 1.2. Gamma Evaluation Method

The gamma evaluation method was first introduced by Low et al. in 1998 and has been widely accepted for comparisons between two dose distributions, where one is defined as the reference information ($D_r(r)$) and the other as the comparison ($D_c(r)$). It is a dimensionless measure and is used in radiotherapy to evaluate the deviation between planned (calculated) and the actual (measured) dose distribution for a given treatment plan.

The method uses the following two acceptance criteria: distance to agreement ($\Delta d_M$) and dose difference ($\Delta D_M$). As a final result, a dose difference distribution is calculated and the regions where the simulated dose distributions disagree with the measurements are displayed. The acceptance criteria is defined by an ellipsoid, in which the boundary represents the acceptance criterion. The equation of the ellipse can be written as:

$$l = \sqrt{\frac{\Delta r^2}{\Delta d_M^2} + \frac{\Delta D^2}{\Delta D_M^2}} \qquad [1]$$

where $r_r$ is the reference point, $D_r$ is the receiving dose at $r_r$, $\Delta r = |r_r - r_c|$ represents the distance between the reference and the compared point and $\Delta D = D_C(r_c) - D_r(r_r)$ represents the dose difference at the position $r_c$ relative to the reference dose $D_r$ at $r_r$. Figure 3 shows a schematic representation of the gamma analysis method for two dimensional dose distribution evaluations.

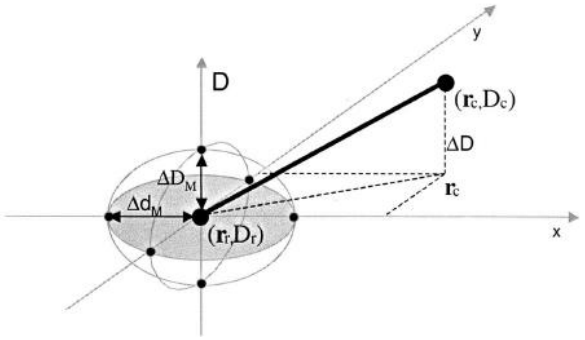


**Figure 3** - Geometric representation of dose distribution evaluation criteria using the combined ellipsoidal dose-difference and distance-to-agreement tests.

A quantitative measure of the method is determined by the gamma value, $\gamma$, which represents the minimum distance between the reference point and the compared distribution:

$$\gamma(r_r) = min\{\Gamma(r_c, D_c)\}\forall r_c \qquad [2]$$

$$\Gamma(r_c, D_c) = \sqrt{\frac{\Delta r^2}{\Delta d_M^2} + \frac{\Delta D^2}{\Delta D_M^2}} \leq 1 \qquad [3]$$

For the dose distribution to match the reference point, it needs to contain at least one point $(r_c, D_c)$ lying within the ellipsoid of acceptance.

The pass-fail criteria leads to:

$|\gamma| \leq 1$, the points meet the acceptance criteria and the points are considered to pass the gamma analyses,

$|\gamma| > 1$, the points do not meet the acceptance criteria and the points are considered to fail the gamma analyses.

The points failing the criteria can be distinguished as points with a higher or lower dose in comparison to the reference point. Positive gamma values represent an increase in dose (hotspots) and negative gamma values represent a decrease in dose (cold spots).

An example of a gamma analysis is presented in figure 4. The color map for the gamma analyses as two transitions at $\gamma$ = 1 and $\gamma$ = -1. The points in the green region are considered to pass the gamma criteria, the points in the red (hot spot) and blue (cold spot) regions are considered not to pass the gamma criteria.

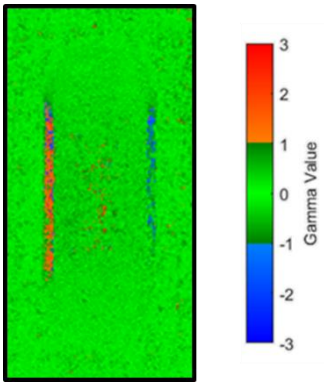


**Figure 4** – Gamma analyses example.

## 1.3. Purpose of the project

Over the past two decades, due to the need of improving dose distribution, radiotherapy underwent through a series of developments where new complex radiotherapy techniques appeared. Meanwhile, these techniques are already implemented in clinical practice without enough experimental validation or strong evidences of its superiority over other techniques. Data based on clinical human trials is difficult to obtain, which makes small animals trials a viable alternative. Although small animal experiments are the best approach, the treatments are mostly based on primitive irradiation techniques. For example the standard treatment utilized to treat small animals uses static single beams often involving partial-body irradiation, which is not representative of what really happens in clinical practice. These differences between the current treatment applied to small animals and the treatments applied in clinical practice present disadvantages for translational knowledge. To better mimic pre-clinical treatments to the ones used in clinical practice more complex treatment plans with more complex or heterogeneous dose distributions are needed. In this way the first aim of this project is to investigate the feasibility of the in house small animal radiation treatment platform (XRAD-225Cx) of delivering complex dose distributions through stage and gantry movement. Treatments based on full stage and gantry rotation allow the delivery of beams from any desired direction and angle which brings a new set of treatment possibilities. Moreover, this project will also investigate if the addition of different degrees of freedom in small animal radiotherapy may lead to improved dose distributions in comparison with the current standard animal treatment.

## 1.4. SmART Group

The SmART group is a group integrated in the Department of Radiation Oncology at Maastro Clinic (Maastricht Radiation Oncology) based in Maastricht, Netherlands. Maastro is an institute that investigates the field of radiation oncology with interdisciplinary clinical, translational and research in physics and biology. The clinic works closely with Maastricht University (UM). The SmART group is focused on the improvement of the acquired small animal research platform (XRAD-225Cx) and development of new techniques which allows increasingly better pre-clinical investigation, enabling the performance of in vivo radiobiological studies in a similar manner to clinical practice. The SmART group works in collaboration with many institutes and groups, particularly with a group named Maastro Lab that investigates the basic mechanism of treatment failure in cancer and tries to apply this knowledge to improve outcome for cancer patients.

## 2. BACKGROUND

In the past few years new irradiation techniques of radiotherapy have been investigated, developed and implemented in clinical practice, which brought an unprecedented level of sophistication in cancer treatment. With the increasing complexity of novel radiotherapy techniques and the need of validation of those techniques, precise small animal irradiators became important to investigate them. In addition, these techniques also allow in vivo radiotherapy drugs experiments on small animals (Butterworth et al., 2014). Many of these novel techniques haven't been properly tested or validated with animal experimental data. The ones tested in animals are mostly based on primitive irradiation techniques only able to administer large radiation fields where a considerable volume of healthy tissues surrounding the tumor are also irradiated. Consequently, these treatments are not representative of what really happens in clinical practice. In this way these techniques have been introduced without solid proof from lab animal experiments to demonstrate their long-term benefit and superiority over less conformal irradiation techniques.

For scientist to understand the mechanism and pathways of cancer and its evolution and spreading over the body and to discover new ways to diagnose and treat cancer it is necessary to carry out experiments on live animals. During studies of radiation effects on tumors and surrounding cells in small animals, there is an increasing need for the development of small animal irradiation devices, which can be capable of targeting and delivering beams in a precise way, especially when investigations include the synergistic effects of different cancer treatments. Due to the advances in technology it is now possible to use radiotherapy approaches for research in small animals, like rats, mice and rabbits. Pre-clinical cancer studies (over 95% of which are conducted on mice) are essential to extend the knowledge and understanding of the mechanisms responsible for cancer and to identify, for example, new targets and biomarkers (Workman *et al*., 2010). Animal studies fall into two broad categories: those using tumor cell transplantation, and those in which tumors arise or are induced in the host. The choice of the animal tumor model depends on the scientific question being investigated. Connecting the existing knowledge of small animal tumor models with the improved small animal radiotherapy platforms the effects of radiotherapy alone or in combination with chemotherapy and/or surgery can be studied with small animals.

Although radiotherapy in small animals may be similar to the modern human radiotherapy process, the size of small animals when compared with humans is largely different. Due to the small size of the animals used for experimental research, their tumors also have a small size. For example a rat brain has an average size between 1.0 cm and 1.5 cm long (Beekman & Vastenhouw, 2004), whereby a brain tumor is even smaller with dimensions in the order of a few millimeters. To have a higher level of treatment accuracy with precise targeting and delivery of high doses a 3D volume sub-millimeter precision is required (Verhaegen et al., 2011). Another major difference is related with the beam energy. In small animal radiotherapy it is necessary to use kilovoltage energy beams instead of megavoltage photon beams as used in clinical practice due to the extent of the dose build up region, which may go beyond the size of the small animal. In this way to avoid extensive disequilibrium dose regions, kV photons between 100 kVp and 300 kVp generated by an X-Ray device are required.

Inherently associated with the accuracy and precision of the treatment in small animals is the image system detection, acquisition and processing. The preferred image modality used in small

animal research platforms is cone beam CT imaging for detection and localization of different structures and treatment planning. The X-Ray detector should have a high temporal resolution and a frame rate of 50 ms for respiratory gating. Due to the size of the animals, micro-CT scanners should acquire voxel volumes with 100 $\mu m^3$.

## 2.1. Small Animal radiation therapy research platforms

Pre-clinical animal experiments have been an essential tool in evaluating the effectiveness of anticancer therapies, studying the underlying mechanisms of disease response, and providing evidence of safety for new drugs and devices. In radiotherapy and radiobiology research, pre-clinical experiments have been used to investigate the response of tumor or normal tissue to radiation exposure, usually with small animals such as mice and rats (Jeong et al., 2015). To overcome these problems, small animal radiotherapy research platforms have been developed by several institutions. There have been numerous publications related to the development of research systems capable of precise irradiation of structures in small animals. Groups from Johns Hopkins University, Princess Margaret Hospital, Washington University, Stanford University and University of Texas Southwestern have either commenced modifications on existing technologies or have developed new ones using their own resources. Among them, there are two relatively mature systems developed independently from Princess Margaret Hospital and Johns Hopkins University.

### 2.1.1. XRAD-SmART

The XRAD-225Cx device was developed at the Princess Margaret Hospital (Canada) in collaboration with the company that commercializes it, Precision X-Ray Inc., and provides in the same platform a high resolution CBCT imaging system and an X-Ray source (5-225KeV). They are both mounted on opposite sides of a C-arm, which rotates $360^o$ for imaging and irradiation, as shown in Figure 5 b) (Verhaegen et al., 2011). In this platform images are acquired in a similar way as they are obtained in clinical practice in which the specimen is stationary and the source and detector rotate around the object. The XRAD-225Cx is enclosed in a cabinet (Figure 5 a)) with two walls of steal and one of lead in-between. It has an inherent collimation and filtration system, manually interchangeable in order to specify the beam size and to deliver the appropriate spectrum for each treatment, respectively. The uncollimated field is a 10 cm x 10 cm square and the available collimators allow a beam size range from 0.1 cm in diameter to 10 cm x 10 cm square. There are two filters presently available, a 2.8 mm aluminum filter and a 0.3 mm copper filter. The system can deliver dose rates of approximately 4Gy/min. To acquire the images, the XRAD-225Cx device has a flat panel detector, consisting of amorphous silicon elements, that is able to image a 10 x10 x 10 $cm^3$ volume with a maximum resolution of 0.1 $mm^3$. The XRAD-225Cx also has an animal stage capable of precise motion in the 3 cardinal directions. The stage has an automated stage correction that corrects for slight motions of the X-Ray tube with respect to the isocenter and the imaging panel during irradiation, which permits a great stability and reproducibility of irradiation. For animal monitoring, 3 webcams are attached in different places inside the cabinet.

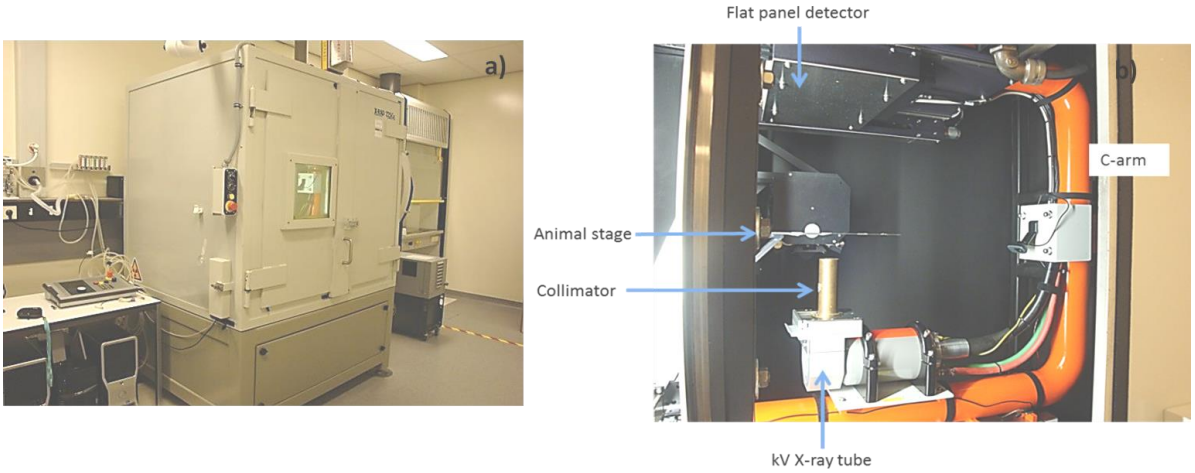


**Figure 5** – XRAD-225Cx device developed at the Princess Margaret Hospital. (a) Cabinet that encloses the XRAD-225Cx device. (b) XRAD-225Cx device and its components.

### 2.1.2. SARRP research platform

The small animal radiation research platform (SARRP) (Wong et al. 2008) developed at Johns Hopkins University and marketed by Xstrahl (Camberley, United Kingdom) integrates a high accuracy cone beam CT imaging system and a high dose delivery X-Ray source in a single platform. The SARRP system and its components are shown in Figure 6 a). The platform consists of a dual-focus constant voltage X-Ray source operating up to 225 kVp, a flat panel detector for target localization, mounted on a gantry with a nominal source-to-isocenter (SID) distance of 35 cm and a robotic stage. This system, like the previous one, can deliver dose rates of approximately 4Gy/min. The gantry can be rotated manually and the rotation is limited from the top to 120° with increments of 15°. To position the animal, computer controlled robotic translation and rotation stages are used. The robotic stage offers 4 degrees of freedom in x and y (cross-table), z (vertical movement) and θ (rotating table). The accuracy of motion in the xy direction and in the z direction is 65 μm and 125 μm, respectively. The accuracy of rotation is 0.05° (Matinfar et al. 2009). Compared with the platforms used in clinical practice, there is an outstanding difference between the SARRP gantry and the one used in clinical practice. In the SARRP system in order to acquire a CT image or to deliver arc beams, instead of rotating the gantry, the stage rotates a full 360° with the gantry at 90°, as shown in Figure 6 b). The SARRP system has an open field size of 20 × 20 cm used for imaging. For irradiation purposes the field can be downsized to a diameter of 0.5 mm due to different manually interchangeable collimators. The SARRP imaging system uses a flat panel amorphous silicon detector with a dimension of 21 cm x 21 cm, which is in the opposite position of the X-Ray source. There are two options for the flat panel detector: 512 × 512 pixel or 1024 × 1024 pixel, providing resolutions of 400 μm and 200 μm, respectively.

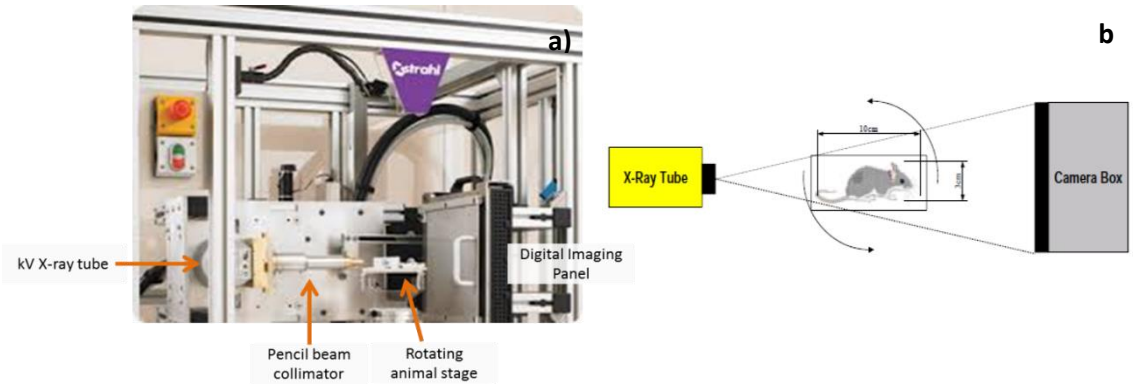


**Figure 6** - (a) SARRP system and the components installed at John Hopkins University with conformal irradiation and cone beam CT guidance capabilities, adapted from (Marchant & Moore, 2014). (b) Representation of the irradiation procedure, where the animal is placed in a rotatable stage between the X-Ray tube source and the detector.

### 2.1.3. SAIGRT system

The small animal image-guided radiation therapy (SAIGRT) is a non-profit academic small animal radiation therapy research platform developed at the Faculty of Medicine and University Hospital Carl Gustav Carus (Dresden, Germany) in collaboration with different institutes. The SAIGRT platform allows for highly precise and accurate conformal irradiation and X-Ray imaging of small animals. It offers a technology comparable to modern human radiation therapy with photons. The platform integrates a 225 kV X-Ray tube used for both imaging and irradiation purposes (Figure 7). By changing the X-Ray source parameters and filtration, the SAIGRT system can provide a wide range of dose rates (<1 $mGy.min^{-1}$ to several $Gy.min^{-1}$) and different photon energy spectra. Furthermore, a digital flat panel X-Ray detector with an active area of 12.32 cm × 11.20 cm and a pixel size of 0.01 cm × 0.01 cm is integrated to perform conventional radiography (CR) and cone beam CT for both treatment planning and animal position verification. The SAIGRT includes an inherent beam collimation system enabling treatments of target volumes with a diameter between 1 and 20 mm allowing for simple, non-conformal (e.g. rectangular or circular) field shapes. Small animal experiments are carried out at the gantry module, which comprises of a 3D computerized stage unit made from 2 mm thick carbon fiber and a 360° rotating arm. The rotating arm carries the X-Ray tube, the system of flat aperture collimators for field formation and the digital flat-panel detector. The device is enclosed by a sandwich aluminium-lead plates with 10 mm thick lead for radiation protection. The system is intended to examine a single anaesthetized small animal.

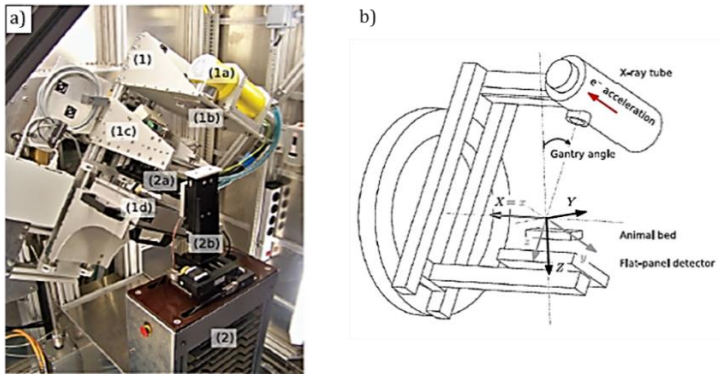


**Figure 7 –** a) Detailed view of the gantry SAIGRT module. Main components are: (1) rotating arm, (1a) X-Ray tube, (1b) primary collimator and filter slot, (1c) secondary collimator, (1d) flat-panel detector, (2) stationary unit, (2a) animal bed, (2b)

animal stage positioner. b) Simplified scheme of the SAIGRT movement components: rotating arm and 3-D computerized animal bed.

### 2.1.4. Small animal irradiator based on GE eXplore RS120 microCT scanner

Besides these previous mature small animal research platforms, there are other platforms under investigation and development. A new small animal irradiator platform was developed by a group at Stanford University (Zhou et al. 2010) based on a GE eXplore RS 120 micro CT scanner. A 2D translation stage and a variable aperture collimator were added to the initial system (Figure 8). The system operates at a tube current between 70 and 120 kVp with a maximum current of 50 mA. The X-Ray tube and the detector panel are placed in opposite sides of the gantry. The platform has a stage system that allows the stage to move along the CT axial direction to carry the animal into and out (z-axis in the CT coordinate system) of the CT scanner for imaging. In order to move the animal in the two other cardinal directions a 2D stage was added (x, left or right and y, up and down). The stage can move 10.2 cm in the z direction, 5.08 cm in the x direction and 2.0 cm in the y direction. A collimation system consisting of two stages, each of them with an adjustable hexagonal iris capable of producing a hexagonal field size between 0.1 cm and 6.0 cm, was added and it is represented in Figure 8 a). The two irises are offset by 30◦ so that when the openings of the two stages are properly adjusted to the same size, a dodecagonal beam profile is formed. This system is capable of deliver dose rates of approximately 2 Gy/min.

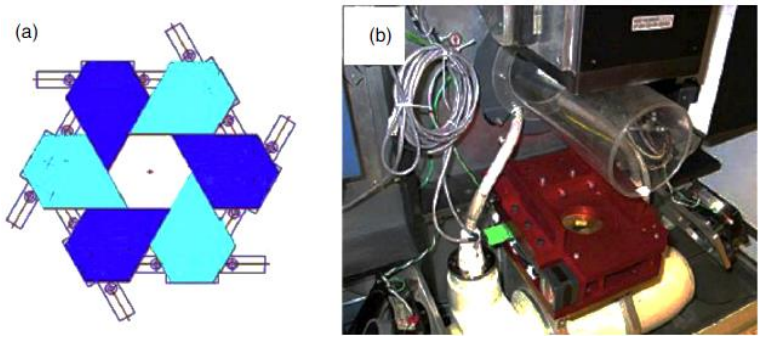


**Figure 8** – Stanford University micro-CT scanner for irradiation of small animals. (a) Representation of the bottom iris collimator formed by six sliding blocks mounted on linear tracks. (b) From bottom to top: X-Ray tube, collimator in its holder, plexi glass CT bore that holds a translation stage and the animal and CT detector. Retrieved from (Zhou et al. 2010).

### 2.1.5. MicroRT—Small animal conformal irradiator

A more basic small animal irradiator was developed at Washington University and this system is drastically different from most X-Ray tube based systems (Stojadinovic et al. 2008) since it utilizes a high dose rate Ir-192 brachytherapy source with a half-life of 74 days and an average gamma-Ray energy of 309 kV as source. As shown in figure 9, the animal can be placed on a three-axis motor stage to move it and the stage is shielded by an aluminum collimator assembly. The aluminum collimator assembly has dimensions of 30.48 cm long, 0.95 cm thick and 15.24 cm outer diameter that holds custom-built tungsten collimators. The stationary beams can be delivered from four directions: 0°, 90°, 180°, and 270°. There are four openings equally spaced on the aluminum collimator assembly that can fit different tungsten collimators providing field sizes of 5 to 15 mm. Once the device has no imaging capabilities, the animal positioning is based on external fiducial markers.

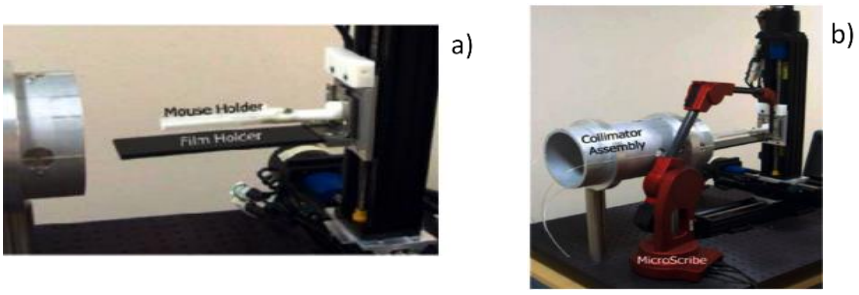


**Figure 9** – Small animal irradiator developed at Washington University. (a) Collimator assembly which can accommodate 192Ir source. (b) computer controlled animal stage in relation to the collimator assembly.

With the exception of the last system, all the previous ones presented here have an integrated anesthetic system based on inhaled anesthesia gas. In the last system the anesthesia is administered by injection.

## 2.2. Treatment planning systems (TPS) for small animals

While the development of micro-irradiator devices had improved the image quality and the irradiation of small structures, a proper treatment planning system (TPS) capable of calculating dose distributions correctly in small structures is needed. Treatment planning is one of the most time consuming phases of a common treatment workflow of small animals treatment as can be seen on Figure 1. A TPS capable of calculating dose distributions is very important not only because it gives information about the dose distribution within the target but also because it gives information about the amount of radiation delivered to regions outside the target. This motivated the development of treatment planning systems that enables the researcher to specify a treatment plan, consisting of one or more beams applied to one or more targets. These treatment planning systems compute the dose distribution and allow the visualization of the resulting dose volume distribution on the structures. Presently, there are two main treatment planning systems being used for small animal irradiations.

### 2.2.1. XRAD SmART-Plan TPS

Recently a TPS called Small Animal Radiation Therapy Plan, (SmART-Plan) was developed by the department of radiotherapy of MAASTRO Clinic (Maastricht, Netherlands) (van Hoof et al., 2013). SmART-Plan was developed in MATLAB, is executed on a Linux-based platform and is based on a robust Monte-Carlo algorithm. The X-Ray device and its collimators are modeled by a photon source from a previous MC simulation (Granton et al., 2012). SmART-Plan allows the user to import the 3D structure of the specimen into SmART-Plan and then the different structures are assigned to different materials according to the Hounsfield Units (HU). The conversion of HU to material type and density is based on a calibration curve. The HU to density calibration curve was constructed based on a phantom with known tissue substitute inserts. Based on a voxel phantom derived from the CBCT scan different structures can be delineated (Figure 10) and targets can be countered. SmART-Plan is capable of simulate static and dynamic beams from a $360^{o}$ arc revolution. As a result of the simulation, SmART-Plan displays 3D dose distributions and dose volume histograms (DVH) of the specified structures. 3D dose distribution and DVH can be optimized by manually adjust the beam weights. SmART-Plan was validated by comparing the calculated absolute depth dose curves and dose distributions in various homogeneous and

heterogeneous phantoms against the measurements obtained with radiochromic film for 1, 5 and 15 mm collimator.

More recently, a group from the department of Econometrics and Operations Research (Tilburg University, Netherlands) in collaboration with the department of Radiation Oncology of Maastro Clinic (Maastricht, Netherlands) developed a framework for inverse planning of beam-on-times for 3D small animal radiotherapy (Balvert et al., 2015). Once the degrees of freedom are increasing the manual creation of beam configurations and dose optimization becomes more complicated and the treatment plan becomes more dependent on the user skills, in this way an inverse treatment planning appears as an important and easier solution for dose optimization. Here, they presented a mathematical model that automatically optimizes beam-on-times. This software is capable of calculating different beam weights based on the specified beams by the user and through an interactive procedure various optimal solutions are generated. In the end, the user can choose the optimal solution. SmART-Plan was used to create beam configurations and perform dose calculations.

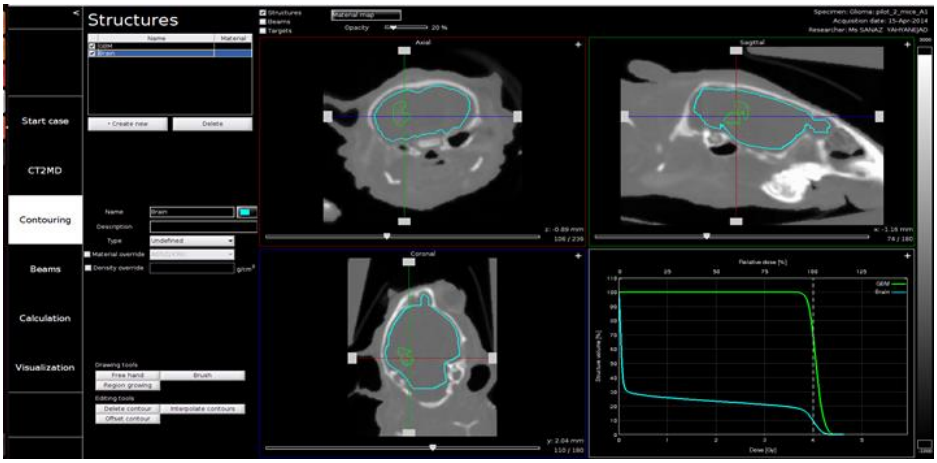


**Figure 10 –** SmART-Plan interface. *Countering* step where the structures of interest are defined and delineated.

### 2.2.2. SARRP MuriPlan TPS

A group from Johns Hopkins University (Baltimore, USA) developed a TPS for the SARRP platform based on the 3D Slicer package (Cho & Kazanzides, 2012), which is an open source application for medical image visualization and analysis (The Slicer Community, 2015). The dose computation was implemented on a graphical processing unit (GPU) to achieve faster processing and it uses the superposition-convolution method to compute dose, rather than Monte Carlo simulation. The TPS module shown in figure 11 a) consists of four stages: Experiment Info, where the images of the animal are uploaded; Target Selection, Treatment Planning (Figure 11 b)), and Treatment Plan Execution. Users are allowed to specify a prescribed dose for each target and create a plan consisting of multiple beam and/or beam arcs. For each entry, the user can specify the isocenter, collimator type, couch and gantry angles, and beam weights. Once a valid plan is created, it can be sent to the dose engine in the SARRP software for execution. The SARRP software receives the plan, and calls the GPU engine to compute a separate dose volume for each plan entry, and then returns the weighted sum of those volumes (i.e., based on the specified beam weights), as well as the exposure time for each plan entry. The SARRP-TPS was validated with 5 different phantom setups (Cho & Kazanzides, 2012). For each setup, a stack of 4 materials with different densities were used. 5 EBT2 films were placed between 5 mm heterogeneous phantom slices.

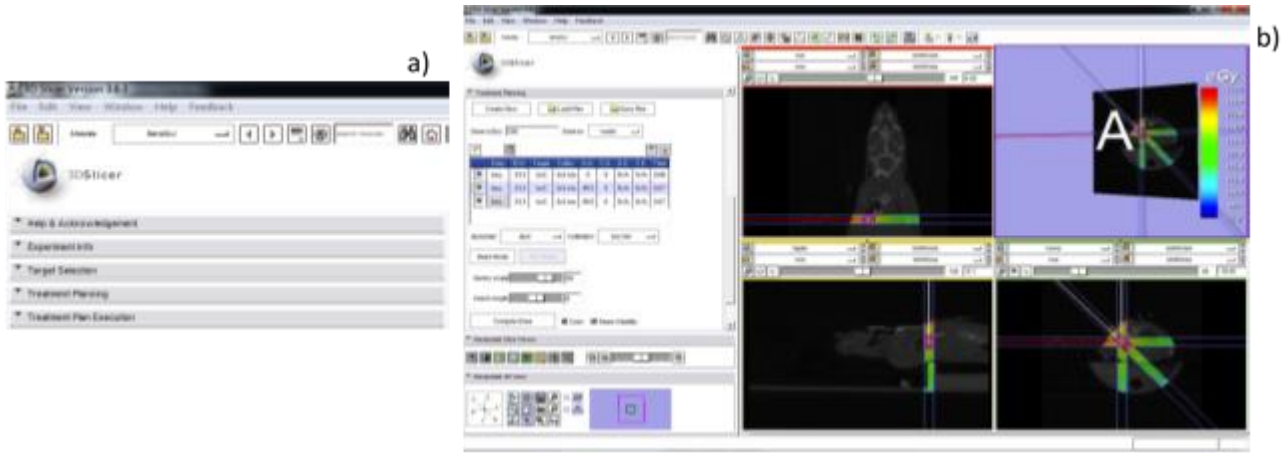


**Figure 11** - SARRP treatment planning system interface. (a) 4 steps of SARRP TPS. (b) SARRP TPS treatment planning step, for a treatmnt with 1 isocenter and 3 beams.

## 2.3. Other developments and studies in small animal radiation therapy

Pre-clinical in vivo studies using small animals are crucial for translational cancer research to develop and optimize therapeutic options of radiotherapy and combined systemic treatment, to examine their efficacy and to investigate side effects. Local irradiation requires reproducible animal positioning, image-guided target localization and accurate beam application to avoid serious side effects when therapeutically relevant doses are being administered using clinically acceptable fractionation schemes. In addition, there is the inherent motion within the animal's body caused by breathing, heart beat or bowel gas (Bartling et al 2008, Kuntz et al 2010, Rubinstein et al 2013) that needs to be taken into account. Despite all the developments made in small animal radiotherapy, research is continuously being made to overcome different technical issues in order to allow more complete and accurate studies.

In pre-clinical radiotherapy when small animals are treated multiple times, reproducibility in inter-fractional treatments is required. To face this problem, a group from Texas University developed 3D-printed immobilization device for mice that allows quick and reproducible small-animal setup (McCarroll et al., 2015). The printed design significantly reduced setup variation, with average reductions in rotational displacement of 76% ± 3% and a translational displacement within the printed immobilizer less than 1.5 ± 0.3 mm.

Gating is necessary in thoracic imaging to prevent a loss of image quality and to acquire 4D data sets. During image acquisition there is a loss in image quality because the acquisition of CT image data takes much longer than the duration of a respiratory and/or a cardiac phase. Image quality is then restricted by the motion of the heart and lung (Bartling et al., 2010). Gating in small-animal imaging requires the acquisition of a gating signal during scanning, which can be done extrinsically or intrinsically from the projection data itself. In extrinsic gating, a motion signal is acquired through an external hardware system for example a camera or a laser system. In this way, the gating signal is used retrospectively during CT reconstruction, or prospectively to trigger parts of the scan. A wide variety of gating methods in small-animal, CT exist and new ones are being developed. The CT scanner type, the scanned animal, and the diagnostic question all have to be taken into account in order to implement gating successfully. The scan protocols, gating parameters and gating algorithms have to be carefully selected and optimized.

In order to deliver treatments based on dose painting, recently a group from Johns Hopkins University (Baltimore, USA) proposed a method to decompose a 2D target in a variable number of rectangles of variable sizes that can be shaped with different collimators (Cho et al., 2014). This method consists of several distinct steps: segmentation, simplification, and decomposition, shown in figure 12, and was implemented on the SARRP treatment planning system. The segmentation step converts the raw image to a 2D label map (i.e., target area) by using the segmentation tool available in 3D Slicer. In the simplification step the label map is approximated to a rectilinear polygon. Finally, in the decomposition step, the rectilinear polygon is decomposed into the minimum number of rectangles possible. Their simulations showed that higher doses occurs primarily at the boundaries between the rectangles, whereby more research needs to be done to investigate this topic. Moreover this prove of concept still needs validation for example with experiments with radiochromic films.

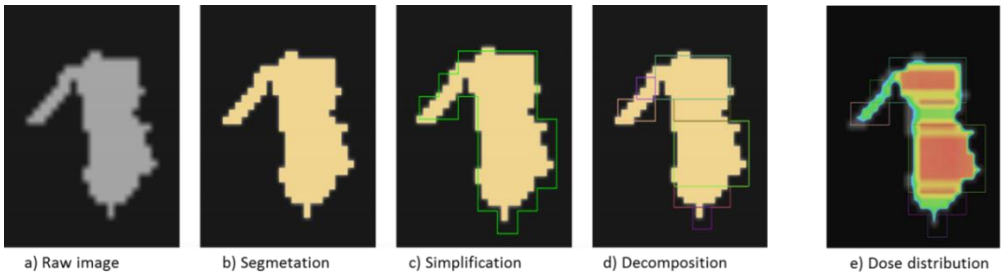


**Figure 12 –** (a) to (d) Different steps of the method developed by a group of Johns Hopkins University to decompose a 2D target in a variable number of rectangles of variable sizes. (e) 2D Dose distribution of the target divided in different rectangles of different sizes computed by SARRP TPS with a beam time of one minute for each rectangular region.

In 2014 a group from the Department of Radiation Oncology at Maastro quantified local changes in mice's lung density by using an image guided small animal irradiator (SmART) for precise irradiation (Granton et al., 2014). In this study they divided 76 adult male mice into 6 groups: a control group (0 Gy) and groups irradiated with single fractions of 4, 8, 12, 16, or 20 Gy using 5 mm circular parallel-opposed beams, targeting the upper right lung. After irradiation, all mice were imaged at regular intervals over 39 weeks. They discovered that mice irradiated with prescribed doses greater than 10 Gy exhibited a steady increase in lung density most pronounced for the 20Gy group, having a maximum difference of 120 HU at the 39th week endpoint compared to the control group. They were also able to show that partial lung irradiation can induce symptoms characteristic of RILF (radiation-induced lung fibrosis) that are discernible as early as 10 weeks post irradiation compared to the nonirradiated group. The data comparison between their results and results from previous pre-clinical studies where large radiation fields, often covering the whole thorax with limited knowledge of where radiation was delivered, were used showed that for the same prescribed dose the severity of RILF in partial lung irradiation in mice can be reduced when a small animal irradiator allowing precise irradiation and the delivery of smaller beams is used.

A study performed by a multidisciplinary team of Ghent University Hospital (Belgium) validated magnetic resonance imaging (MRI) as a possible choice as image modality for guided micro-irradiation for the F98 glioblastoma rat model using SARRP (Bolcaen et al., 2014). MRI images were used to define the target and the CBCT was used to calculate the dose plan. In the study 10 rats were inoculated with F98 tumor cells in the right frontal hemisphere and then were treated by combining radiotherapy with temozolomide (oral chemotherapy drug). Four different radiotherapy treatment protocols were applied, all of them with a delivered dose of 20 Gy to the

tumor volume. In the first treatment only the on-board CT for imaging was used for delineation and dose planning. In this treatment a single static beam was delivered with a width of 10 mm, once the tumor was not visible. For the other 3 remaining treatments an MR image was used to delineate the tumor, which allowed the use of a 3 mm x 3 mm collimator. With the tumor delineated dose plans for a single beam, a single arc and 3 non-coplanar arcs were delineated. The comparison of the different treatment plans showed that the homogeneity of the dose distribution increases from a single static beam, a single beam arc and three non-co planar arc beams. The results also showed that the most important difference between using a single CT-guided beam and a MRI-guided beam is the low dose delivered to the normal brain tissue when MR images are used for delineation, with the three non-coplanar arcs beams MRI-guided treatment being the one that delivers less dose to the normal brain. Using the approach with the SARRP and concomitant TMZ, tumor growth was stable until 9 days post-irradiation, while tumors in the control group showed rapid proliferation.

# 3. MATERIALS AND METHODS

## 3.1. SmART X-Radiation platform

The small animal research platform used at MAASTRO Clinic is the XRAD-225Cx device (Figure 13). The specifications of the irradiation, imaging and hardware of SmART platform are presented on Table 1.

**Table 1 –** Overview of the properties of the XRAD-225Cxplatform according to the manufacturer. Adapted from (van Hoof, 2012).

| | | |
|---|---|---|
| **Geometrical setup** | | |
| Source to detector distance (SDD) | 645 mm | |
| Source to isocenter distance (SID) | 307 mm | |
| **Irradiation** | | |
| Energy | 5 - 255 kVp | |
| Dose rate | up to 4 Gy/min | |
| Beam Orientation | fixed and/or dynamic 0 to 360 degrees | |
| Interchangeable filtration | 2.0 mm Al and 0.32 mm Cu | |
| **X-Ray Power Supply** | | |
| Max output voltage | 225 kV | |
| Max output current | 45 mA | |
| Max Output Power | 45 kW | |
| **X-Ray tube** (Unipolar Metal Ceramic Tube) | | |
| Nominal Operating Voltage | 225 Kv | |
| Inherent Filtration | 0.8mm Be | |
| Target Material | Tungsten | |
| **Collimators** | **Circular** | **Rectangular** |
| beam size (mm) | 1.0 | 10 x 10 |
| | 2.5 | 20 x 20 |
| | 5.0 | 30 x 30 |
| | 10 | 40 x 40 |
| | 15 | 10 x 30 |
| | 25 | 30 x 40 |
| **Animal Stage** | | |
| Load capacity | 4.5 kg | |
| Positional accuracy | 82 µm | |
| Stage speed | up to 36mm/s | |
| Maximum Travel | Lateral (x) | 184.47 mm |
| | Longitudinal (z) | 129.71 mm |
| | Vertical (y) | 180.92 mm |
| **Gantry** | | |
| Gantry speed | 0.01 to 3.0 RPM | |
| Positioning accuracy | < 6 arc per minute | |
| **Imaging detector** (silicon flat panel) | | |
| Active pixels | 1024 x 1024 | |
| Pixel pitch | 200 µm | |
| Total Area | 20 cm x 20 cm | |
| Maximum frame rate | 30 fps | |

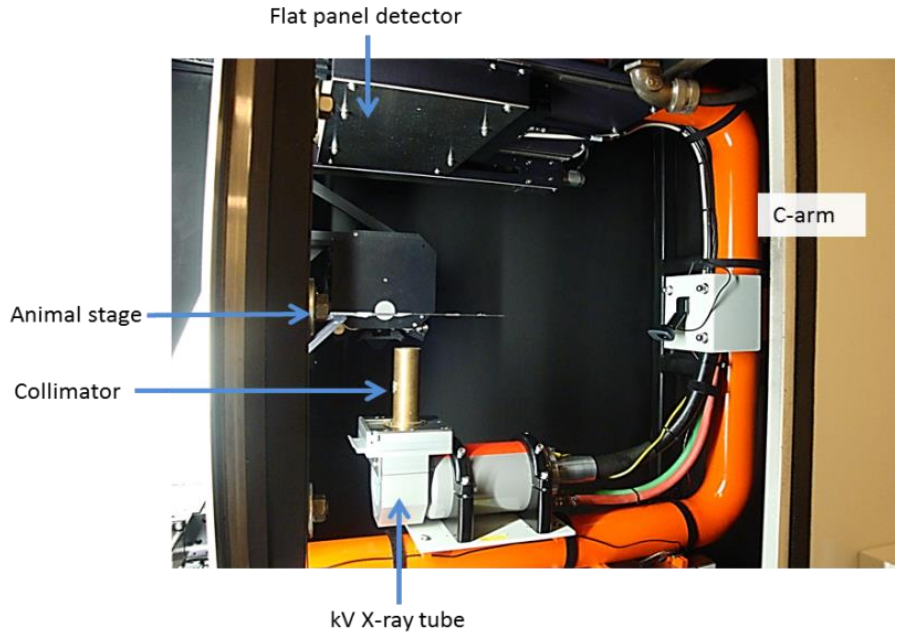


**Figure 13 -** XRAD-225Cx platform installed at MAASTRO Clinic and its components. The X-Ray tube (bottom, white) is supported by the C-arm (orange). On the top of the C-arm is visible the cone beam CT imaging panel (dark gray). In between the CT imaging panel and the X-Ray source is located the 3D computer-controlled animal stage.

### Pilot workstation and Pilot treatment protocol

To be able to access the CBCT acquired images, deliver the treatment plan, guide the targeting system and control system calibrations a user interface is needed. In the case of the XRAD-225Cx the software responsible for this, is a control software called Pilot, which was developed at Princess Margaret Hospital (Canada). Both of them are provided by the small animal facility at MAASTRO Clinic. Through this main user interface, the user has access to the CBCT acquired images of the specimen, which allows him to choose and fix the target isocenter that can be selected by moving the stage to the right position (Figure 14). Scans and treatments are organized in a searchable database by researcher and study. Since a high resolution CBCT scan of a large volume is time and memory consuming, firstly a CBCT with low resolution is acquired for gross overview of the specimen and afterwards a high resolution CBCT scan is done in a smaller selected region of interest. The treatment plan is based on the acquired CBCT data and for each treatment a protocol is generated as a text file. Pilot receives the treatment protocol and XRAD-225Cx executes it, delivering the proper treatment by irradiating the target as specified in the text file.

A treatment protocol is a structured text file that describes a sequence of steps, motions, irradiations, beam angles and other variables needed to deliver a proper treatment. A treatment protocol consists of a number of beams and each one of them is divided in control points (CPs). A CP is the representation of the machine state in a specific moment of time. For each CP can be specified the stage position, the beam angle, the gantry rotation direction and respective delivered dose. The dose is delivered in a segment between CPs and is measured as “seconds of beam-on-time”. Thus the dose is measured according to the time that the beam is on. An example of a treatment plan protocol can be found in appendix A.

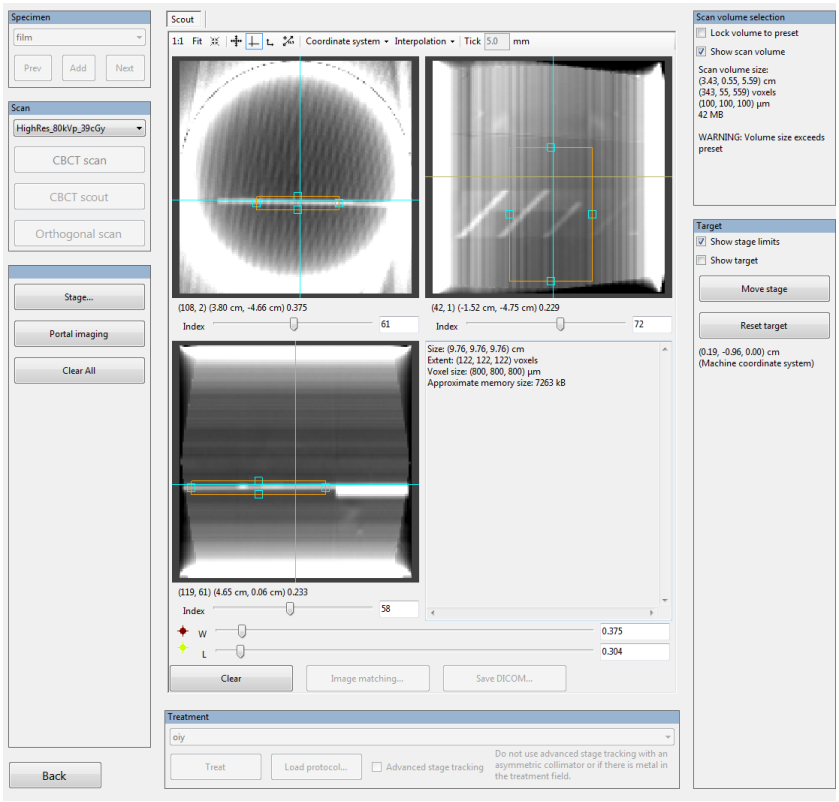


**Figure 14 –** Pilot interface displaying a low resolution CBCT data in the axial, sagittal and coronal planes. It can be seen in orange the selected region to acquire the high resolution CBCT scan.

## 3.2. Treatment Planning System

SmART-Plan is the TPS associated to the XRAD-225Cx platform. It is divided in six different sections (Figure 15). In the first section, *Start case*, the CBCT data is imported as a DICOM file. In the *CT2MD* section the different structures are assigned to the corresponding material. In the *Contouring* section the user can delineate and specify the important structures to be irradiated or to be avoided. To calculate the dose distribution the user needs not only to add a target and the prescribed dose, but also to specify the number of beams and beam angles used (*Beams* section). After the user specifies the number of generated particles per beam, the treatment is simulated in the *Calculation* section. When the simulation is over, SmART-Plan displays a 3D dose volume distribution and the DVH for the specified structures in the *Visualization* section as it can be seen in Figure 15. In this section the user can also change the beam weights and new dose volume distributions and DVH are generated.

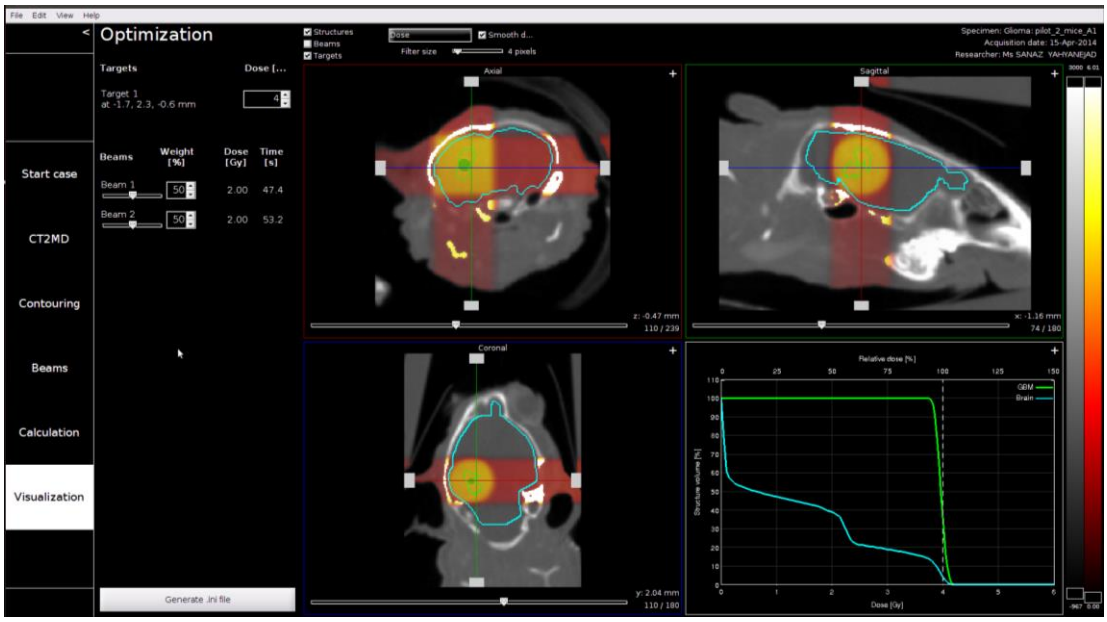


**Figure 15 -** SmART-Plan interface. *Visualization* section where the 3 different views (axial, sagittal and coronal) of dose distribution and DVH are displayed for two structures, a mouse tumor (target) and the brain (minus target).

## 3.3. EBT3 films

A verification process to evaluate real delivered doses is needed and radiochromic films appeared as a relevant tool to assess dose distributions. In particular, Radiochromic EBT3 film (Ashland Inc) was accepted by the scientific community as a reference two-dimensional detector. The EBT3 film is made by laminating an active layer with a yellow marker dye between two polyester layers with equal thicknesses (Figure 16 a)). Radiochromic EBT3 film changes its color when exposed to radiation and the amount of color change is dependent on the dose it receives (Figure 16 b)). When the film is irradiated, the ionizing radiation initiates a polymerization process in the active layer that changes the optical absorbance. By digitizing the film using a document scanner, it becomes possible to access the optical density with respect to the dose. To convert the response of the radiochromic film (change in optical density) into absolute dose, a calibration curve is needed. EBT3 film is an important tool to access the dose due to its high spatial resolution, energy-independent dose response from the kV to the MV range, as well as its near-tissue equivalence.


Figure 16 – (a) Radiochromic EBT3 film structure with different layers of different materials and different thicknesses. (b) Color change of a piece of a Radiochromic EBT3 film after irradiation.

## 3.4. Stage positioning validation

To be able to deliver heterogeneous dose distributions by using stage motion during irradiation it is extremely important to assess the performance, the accuracy and the stability of the animal stage. To measure the animal stage movement, an ultra-sound (US) system was used (BALLUFF, BUS RO04K) (Figure 17). The specifications of the US sensor are presented in Table 2. The time resolution of the US sensor was set to 12 ms for all the measurements.

**Table 2 –** Specification of the Ultra Sound sensor to evaluate the SmART animal stage.

| | |
|---|---|
| Blinding zone | 0 – 20 mm |
| Operating scanning range | 20 – 150 mm |
| Limiting scanning range | 250 mm |
| Resolution | 0.056 mm |
| Response time | 24 ms |

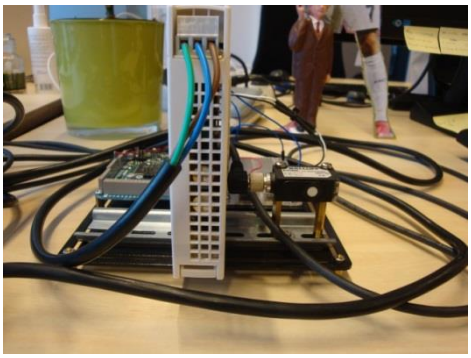

**Figure 17 -** Ultra-sound system used to evaluate the animal stage of the XRAD-225Cx (Precision X-Ray, CT, North Branford).

### 3.4.1. Calibration and validation of the US sensor

As a first step and before evaluating the stage positioning, a validation of the US system was needed. To validate it, a dynamic thorax phantom "CIRS" (Universal Medical, model #008A) was used (Figure 18).

The CIRS phantom is a precision instrument used to investigate the impact of tumor motion inside the lung and patient positioning errors in radiation therapy. The phantom body represents an average human thorax in shape, proportion and composition. A major component of the dynamic system is the precision motion actuator. The three-dimensional motion to the tumor in the phantom body is achieved by the actuator which applies synchronized linear and rotational motion to a moving rod. Sinusoidal and other complex motions can be achieved with sub-millimeter accuracy and reproducibility. The CIRS phantom allows simulations of sinusoidal movements, for which the amplitude and period can be specified. With the amplitude and period defined, the periodic movement was measured with the US system and was compared to the sinusoidal movement of the CIRS phantom. As the output of the US sensor is an analog signal, an ADC (Analog to Digital Convertor) is needed to convert the analog signal (voltage) to a digital number. To smooth the ADC signal (digitalized value of voltage) an average filter was used. The average filter used was based on a filter, where the ADC value that is being filtered is replaced by the mean ADC value of the four previous ADC values including itself. Once the output of the US system is in ADC values, a calibration is needed to convert the ADC values to distance. To calibrate

the US system a regular ruler was used and an object was translated over a distance of 5 cm in steps of 0.5 cm. The ADC signals were acquired during 6 seconds for each distance (Figure 19) and their mean (for each distance) were calculated. Using the mean ADC values for each distance a linear calibration function of distance as function of the ADC values was created.

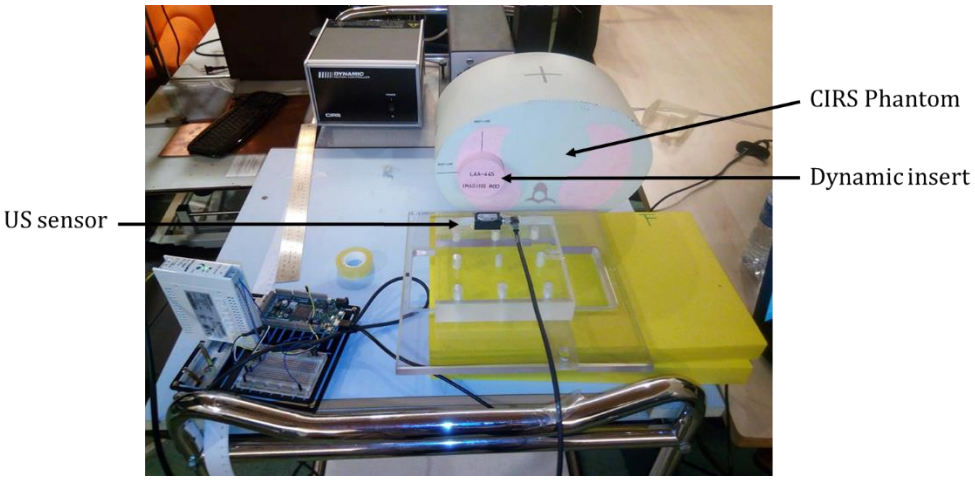


**Figure 18 –** Experimental setup used to validate the US system. The US system was validated with the dynamic thorax phantom "CIRS" (Universal Medical, model #008A).

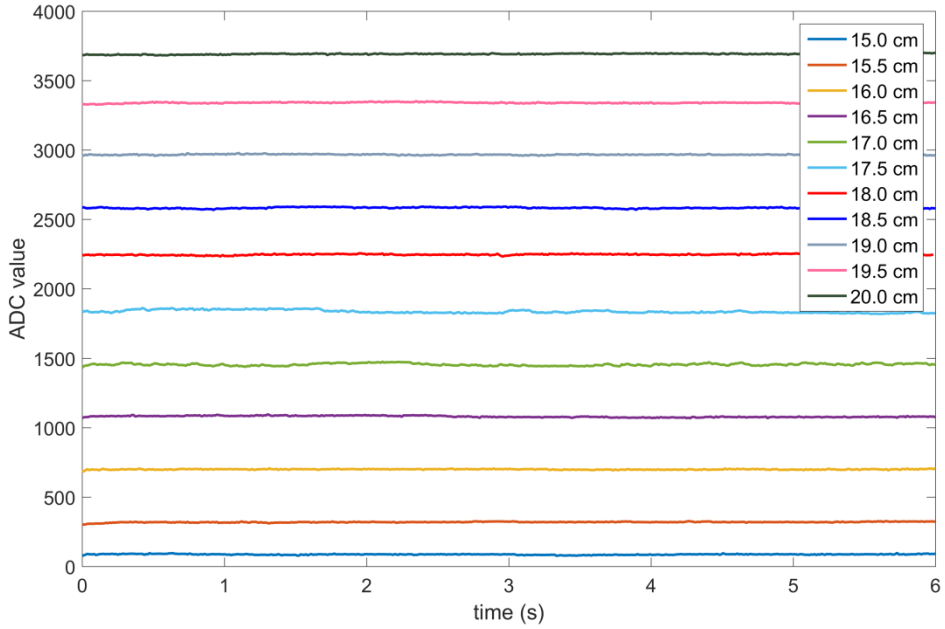


**Figure 19 –** Acquired ADC values for 11 different distances spaced 0.5 cm from each other during a period of 6 seconds with the US system. The ADC values for each distance were used to create a calibration function to convert the output of the US system in ADC values to distance.

### 3.4.2. Stage translation validation

To measure and evaluate the stage motion in the longitudinal (z axis), lateral (x axis) and vertical (y axis) directions, protocols with different numbers of CPs, 5, 10, 20, 50, 100, 150 and 180, were created. The experimental setup used to measure the stage movement in the different directions is represented in Figure 20. The total stage movement was kept constant at 2 cm for all the 3

directions and the irradiation time was 120 seconds. The longitudinal stage movement was also measured for a beam-on time of 60 seconds and a translation of 3 cm.

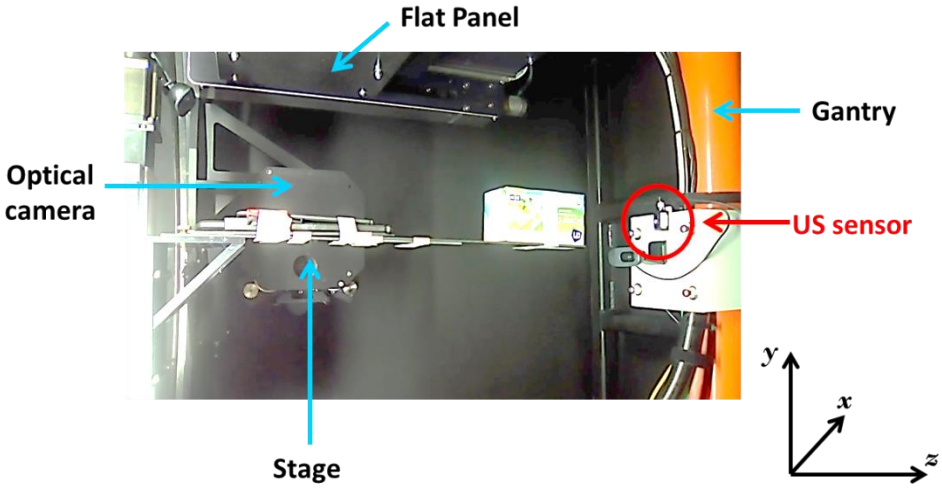


**Figure 20 –** Experimental setup for the US measurements. To measure the stage movement in the longitudinal direction (z axis), the US sensor (in red) was attached to the gantry, to measure the stage movement in the lateral direction (x axis) the US sensor was attached to the optical camera and to measure the stage movement in the vertical direction (y axis) the US sensor was attached to the flat panel detector. The US sensor position is stationary and the reflective object, represented by the box, was attached to the moving stage.

The stage speed between CPs was also evaluated for the different directions for a stage translation of 2 cm and an irradiation time of 120 seconds. The stage speed was calculated for one case, 10CP. For higher numbers of CPs the steps between CPs were not discernable anymore. The stage speed was calculated based on the data acquired with the US system. Figure 21 shows that the steps that represent the stage movement between CPs are clearly distinguishable for 10 CPs. The speed of the stage for each step is given by the slope (m) of the regression function (black solid line): $distance = m * t + b$, as shown in Figure 21. For each step a different regression function needs to be calculated.

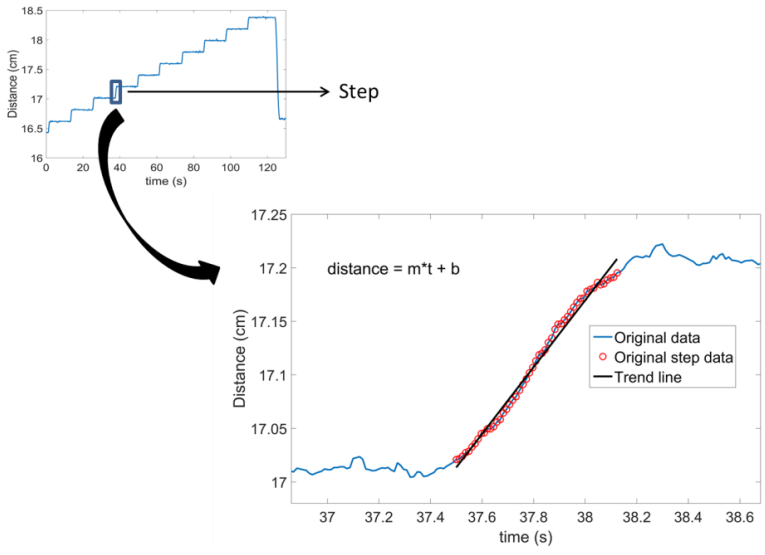


**Figure 21 –** Representation of a step of a stage translation of 2 cm and an irradiation time of 120 seconds for 10 CPs. The data was acquired with the US system and each step represents the stage movement between CPs. For each step a different regression function is calculated and the slope (m) of each regression function gives the speed of the stage for the different steps.

## 3.5. Homogeneous dose distributions

### 3.5.1. Required distance between CPs

It is known that increasing the number of beams used in the treatment plan increases the homogeneity of the dose distribution (Motomura et al., 2010). Here, the required spatial separation between CPs was studied with the aim of mimicking a homogeneous dose distribution for 3 circular fields with diameters of 2, 5 and 10 mm. For each field dimension, cases with different numbers of CPs were simulated, with a total stage translation of 2 cm for the 5 and 10 mm circular beams, and a total stage movement of 1 cm for the 2 mm circular beam. To evaluate the dose homogeneity, the standard deviation of a region of interest in the central region of the dose distribution was calculated. A region of interest for a beam size of 10 mm is represented in figure 22. Different regions of interest dimensions were considered for the 3 different fields. Regions of interest of 0.0425 $cm^2$, 0.1214 $cm^2$ and 0.3192 $cm^2$ were considered for the 2 mm, 5 mm and 10 mm circular beams, respectively.

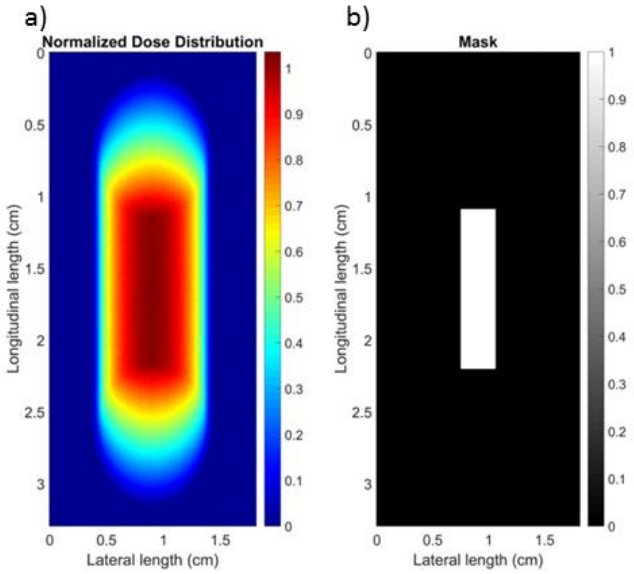


**Figure 22** – a) Dose distribution for the 10 mm circular beam using 100 CPs. b) Mask used to define the region of interest.

The required number of CPs (#CP) can be calculated using equation 4.

$$\#CP=\text{round}\left(\frac{\text{Total Distance}}{\text{Space between CP}}\right)+1 \qquad [4]$$

### 3.5.2. Evaluation of dose distribution during irradiation

In this section the possibility of delivering complex dose distributions using the XRAD-225Cx platform was investigated. As a first step the stage motion was studied while the gantry was stationary. Following this and as a second step, simultaneous stage and gantry movement during irradiation was studied.

#### 3.5.2.1. Stage translation & Stationary gantry

The evaluation of the stage translation, while the gantry was stationary, was based on dose distributions. To assess the dose distributions, radiochromic EBT3 films (Ashland, Lot # 04151402) were placed on the animal stage perpendicularly to the beam. The EBT3 films were scanned 24 hours (enough time for the polymerization process occurs) after irradiation using an Epson Perfection V750 Pro flatbed scanner and the Epson Scan software v3.83 (Seiko Epson Corporation, Nagano, Japan). Each film was scanned separately in the center of the scanner. The scanned images were saved as triple channel (Red-Blue-Green) TIFFs with a spatial resolution of 225 DPI and an intensity resolution of 48 bit (16 bit per color channel). For each image the optical density was converted to dose using the triple channel method (Hoof, 2012). Dose distributions were evaluated for dose delivery plans using 20, 50, 100, 130, 150 and 180 CPs, for longitudinal and for lateral stage translations. Different treatment protocols were created with a total stage translation of 2 cm and an irradiation time of 120 seconds. To compare the dose distribution between the longitudinal and lateral stage translation the gamma analyses method was used with a dose difference criteria of 3% and a distance to agreement criteria of 0.5 mm.

#### 3.5.2.2. Stage translation & Gantry rotation

To investigate the simultaneous movement of the gantry and the stage in the longitudinal direction, protocols with 25, 50 and 100 CPs were created. Protocols with 25, 50 and 100 CPs were created to evaluate the feasibility of delivering complex dose distributions based on treatment plans with low and high number of CPs. For each protocol the number of CPs used for the translational movement was the same used for the gantry movement. The stage movement was fixed to 2 cm, the irradiation time was 200 seconds and the gantry rotation was set to one full rotation per treatment protocol. The dose distributions were measured with radiochromic EBT3 films (Ashland, Lot # 04151402). The EBT3 films were placed between 2 slabs of water equivalent material in parallel to the stage.

To evaluate the different delivered treatments, the delivered (measured) dose distributions were compared with simulations through the gamma analyses method. For the treatments where the stage was moving but the gantry was stationary, the simulations were based on CBCT images with an isotropic voxel spacing of 0.2 mm. For the treatments where both stage and gantry were moving simultaneously, the simulations were based on CBCT images with an isotropic voxel spacing of 0.1 mm. The simulations were performed using SmART-Plan. The gamma criteria used for the comparison in the first case was a dose difference of 3% and a distance to agreement of 0.5 mm. The gamma criteria used for the comparison for the second case was a dose difference of 5% and a distance to agreement of 1.0 mm. A circular field with a diameter dimension of 10 mm was used for both cases.

## 3.6. Need of additional spatial degrees of freedom in small animal radiotherapy

Rotating the stage in the xz plane and the grantry in the y plane (figure 23 a)) enables the delivery of beams from any desired angle.

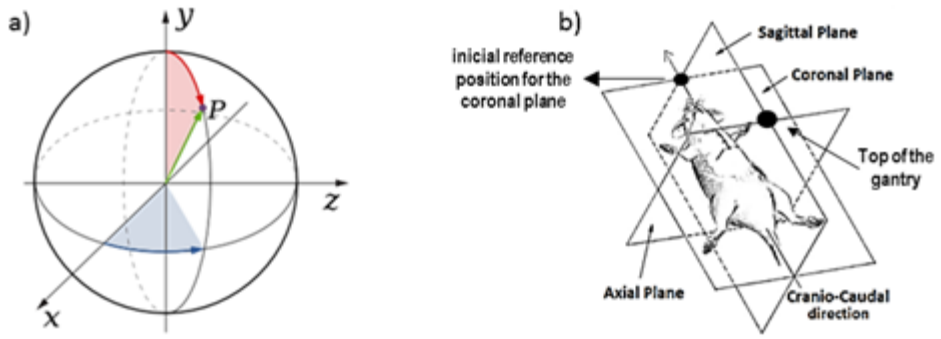


**Figure 23 –** a) Spherical coordinates. b) The three orthogonal anatomic planes of the rat body.

To assess if beams delivered from different directions in small animal radiotherapy improve dose distributions, two different cases were considered. The treatment plans were based on CBCT images with an isotropic voxel spacing of 0.1 mm. For the two cases a prescription dose of 4 Gy to the tumor was used. In both cases, treatment plans with different beam configurations were simulated and all the treatments were scaled to the same $V_{95\%}$ of the tumor. Here, $V_{95\%}$ is defined as the fraction of the tumor volume receiving at least 95% of the prescribed dose. Circular beams with a diameter of 5 mm were used for the simulations and the beams were linked to the same machine isocenter for all the different treatment cases. Treatment plans were evaluated based on DVHs and Dose-Volume (DV) metrics, $D_{mean}$, $D_{max}$, $D_{5\%}$ and $D_{1\%}$. The simulated treatment plans with beams delivered from different directions were compared with a standard treatment plan used in current pre-clinical practice, which is usually done with one or two beams delivered from the axial plane (rotating gantry axis) (Figure 23 b)).

### 3.6.1. Mouse Glioblastoma case

The first case consisted of a mouse glioblastoma where only two structures were considered, the tumor and the normal brain tissue, since the lack of imaging contrast between tissues made the tissue segmentation nearly impossible. The first treatment plan consisted of two parallel opposed beams (considered standard treatment). For the second treatment plan, a full 360 degree arc in the axial plane was simulated. In the third treatment case, a beam configuration consisting of a beam rotated 60 degrees from the axial plane in the cranio-caudal direction was considered.

### 3.6.2. Mouse Right Lung tumor case

The second case was a tumor located in the right lung of a mouse. In this case seven organs at risk located in the thorax were considered. The delineation of the tumor and the organs at risk was made by a qualified radiation oncologist. Three treatment plans with different beam configurations were simulated. The first treatment case consisted of two beams delivered in the axial plane. One of the beams was positioned 9 degrees from the vertical axis and the other beam was positioned at -99 degrees from the vertical axis. In the second beam configuration, three beams were positioned at 30, 40 and 50 degrees from the axial plane in the cranio-caudal direction. For the last treatment case eleven beams were delivered from multiple directions.

Specific information about the number of beams, beam angles and beam directions used per treatment case can be found in Appendix C.

## 3.7. Treatment based on stage translation

As a final step, a treatment based on stage movement for a real mouse case with a tumor in the right lung, where 7 structures at risk were considered, was simulated. To simulate a treatment based on stage movement the beam size has to be smaller than the target.

To define the different stage positions, as a first step, the slices in the z direction (axial slices) containing the target structure (i.e. tumor) are selected. After all the z positions are selected and based on the contours of the target structure, a grid with the x and y positions per slice is created for each axial slice, originating a x, y and z value for each stage position (figure 24). The treatment plans simulations were based on CBCT images with an isotropic voxel spacing of 0.1 mm.

A treatment plan based on stage translation was compared with a similar treatment plan based on a single stage position with a beam size bigger than the tumor. For the case based on stage translation 316 different stage positions were considered, with a beam of 2 mm being delivered from the top. For the case based on a single stage position, a configuration of two beams was considered where one beam was delivered from the top and the other one was deviated 5 degrees from the vertical axis. To collimate the beams, a circular field with a diameter of 5 mm was used. For the two simulations a prescription dose of 4 Gy to the tumor was used and both treatments were scaled to the same $V_{95\%}$ of the tumor.

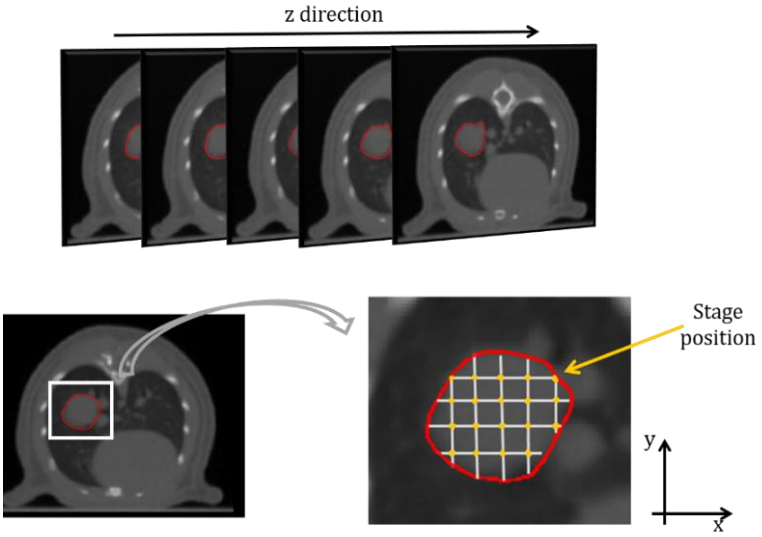


**Figure 24 –** Schematic representation of the process to define the different stage positions of a treatment based on stage movement for a mouse tumor case. As a first step slices in the z direction containing the target structure (red structure) are selected. After all the z positions being selected and based on the contours of the target structure a grid with the x and y positions per slice is created for each axial slice, originating a x, y and z value for each stage position.

Specific information about the number of beams, beam angles and beam direction used per treatment case can be found in Appendix D.

# 4. RESULTS

## 4.1. Stage positioning validation

### 4.1.1. Calibration and Validation of the US sensor

Measured calibration data and the fitted calibration function of distance as function of ADC values are both presented in figure 25. Blue circles indicate the mean ADC values acquired with the US system for all calibration distances. The resulting equation for the linear fit is:

$$Distance = 1.35 \times 10^{-3} * ADC + 15.01 \quad [5]$$

where distance is in cm. The high value of the $R^2$ indicates that the calibration function fits well to the calibration data with low residual values.

The theoretical sinusoidal movement of the CIRS phantom and the movement measured with the US system are plotted in figure 26. The amplitude of the sinusoidal movement of CIRS phantom was defined to 1.5 cm and the period of the movement was set to 4 seconds. The results indicate a good overlap between the theoretical sinusoidal translation and the translation measured with the US system, indicating a trustful measurement of a real dynamic translation.

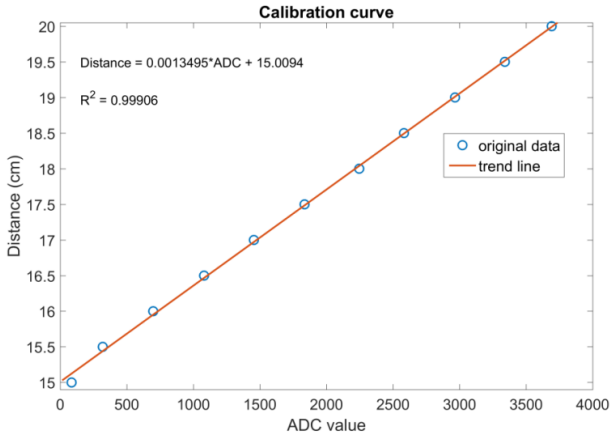


**Figure 25** – Calibration curve and fitted linear equation to convert the acquired signal with the US system in ADC values to distance in cm. Blue circles represent the mean ADC values for each distance and the red line represents the fitted linear function.

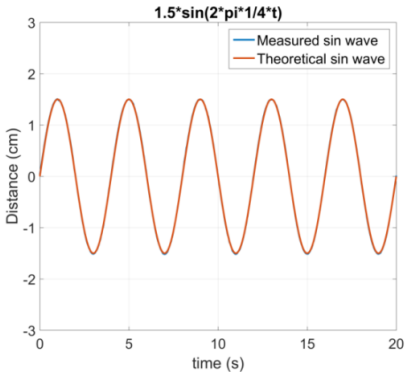


**Figure 26 –** Validation data for the US system. Representation of the (red) measured inserted sinusoidal wave with an amplitude of 1.5 cm and a periodic movement of 4 seconds and (blue) the measured sinusoidal wave with the US system.

### 4.1.2. Stage translation validation

Figure 27, 28, and 29 show the stage translation measurements for the longitudinal, lateral and vertical directions, respectively, obtained with the US system for 5, 10, 20, 50, 100, 150 and 180 CPs. For a small number of CPs (up to 20), the distance between CPs is higher making the CPs distinguishable. For higher numbers of CPs, the stage translation resembles a continuous translation.

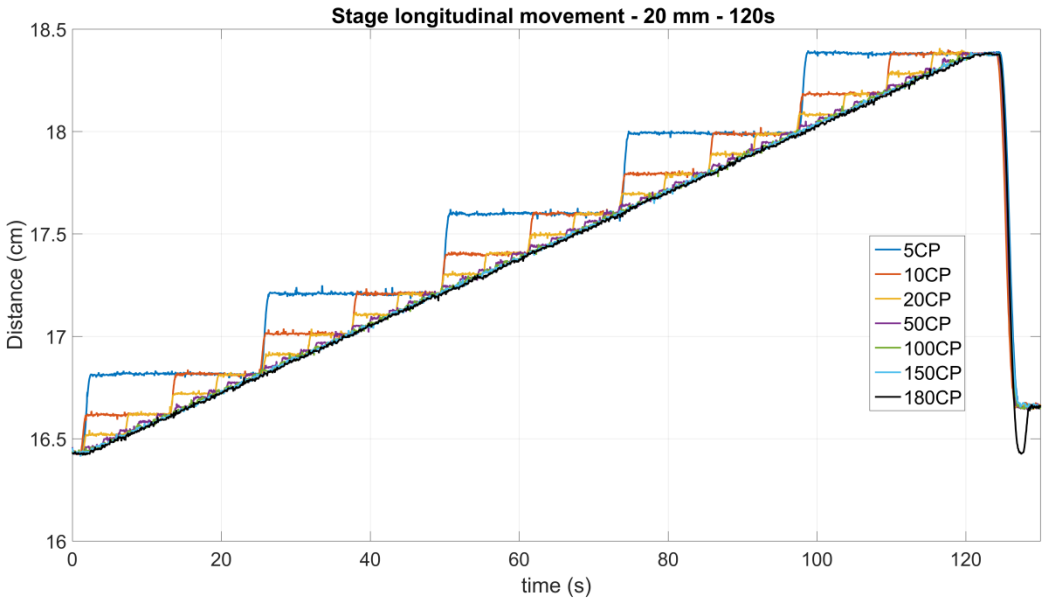


**Figure 27** – Stage translation in the longitudinal direction for different numbers of CPs. The stage position was measured with the US system and the total distance was set to 2 cm for an irradiation time of 120 seconds.

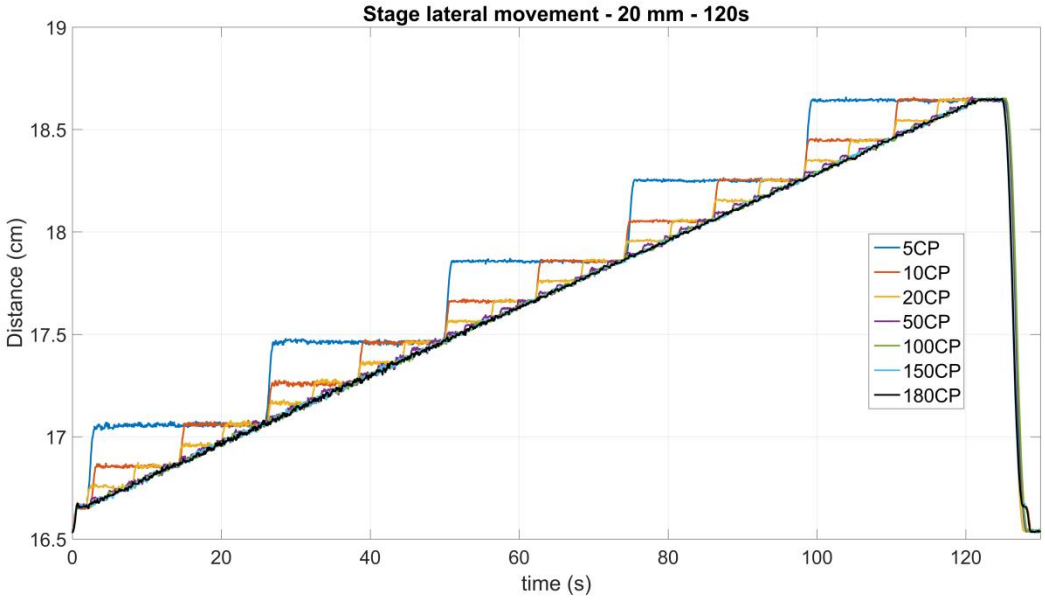


**Figure 28 -** Stage translation in the lateral direction for different numbers of CPs. The stage position was measured with the US system and the total distance was set to 2 cm for an irradiation time of 120 seconds.

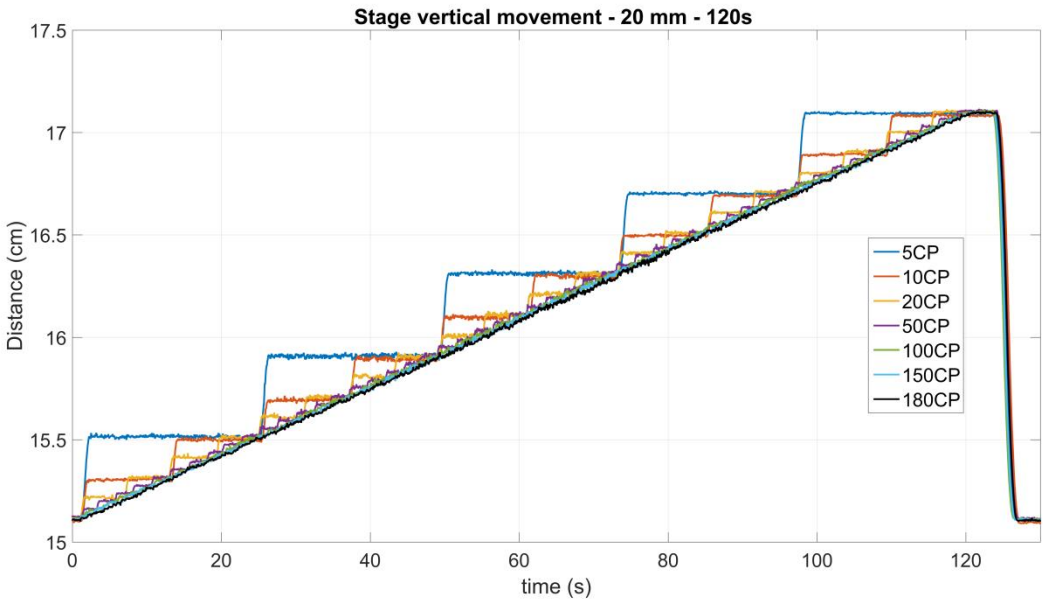


**Figure 29 -** Stage translation in the vertical direction for different numbers of CPs. The stage position was measured with the US system and the total distance was set to 2 cm for an irradiation time of 120 seconds.

The total stage translation measured for different numbers of CPs for each direction is presented in figure 30 a). Each line represents the mean total stage translation for the different directions. The mean total stage translation was 1.949 ± 3.848*10$^{-03}$ cm, 1.988 ± 5.350*10$^{-03}$ cm and 1.985 ± 4.504*10$^{-03}$ cm for the longitudinal, lateral and vertical direction respectively. Coefficients of variance (COV) were calculated for the stage translation in the different directions. COVs indicate the ratio between the standard deviation of the total stage translation and the mean for the different numbers of CPs. The coefficient of variance for the stage translation in the longitudinal direction was 0.20%, 0.27% for the lateral direction and 0.23% for the vertical direction. The obtained low COV values indicate that the stage translation is not dependent of the number of CPs used.

Figure 30 b) shows the total stage translation error per number of CPs for the three directions. The error was calculated between the total measured translation and the one specified in the protocol, 2 cm, for the different numbers of CPs. The lines represent the mean error of the stage translation for each direction. The longitudinal direction showed the highest mean error, which was 2.56% compared to mean errors of 0.62% and 0.77% for the lateral and vertical direction, respectively. Among all the directions and numbers of CPs, the stage translation error was always below 3%, suggesting that the stage reproduces well what is specified in the protocols.

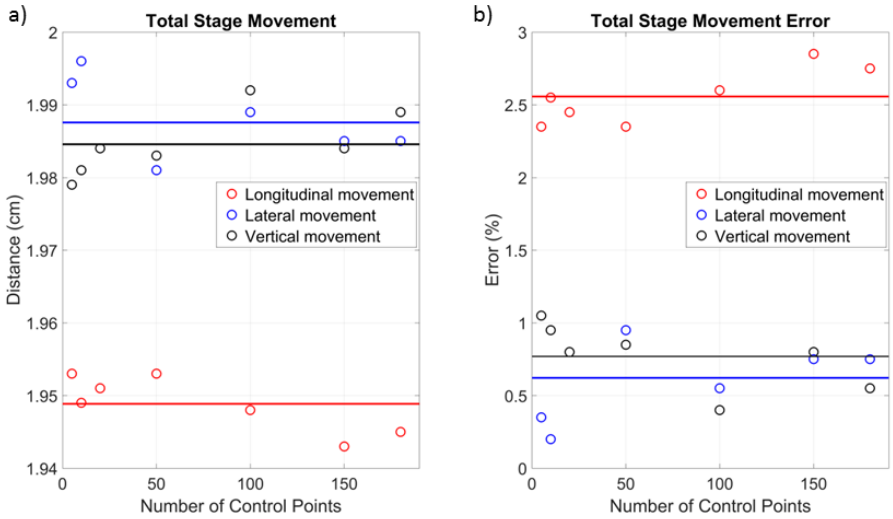


**Figure 30 –** a) Total measured stage translation for different numbers of CPs in the 3 different directions. The lines represent the total mean stage translation for each direction. b) Total stage translation error for the different CPs for the 3 different directions. The lines represent the mean stage translation error value in each direction.

## Stage speed

The mean stage speed per step for the longitudinal, lateral and vertical directions for 10 CPs is shown in figure 31. The horizontal lines represent the mean stage speed for each direction. The mean stage speed translation in the longitudinal direction was 0.332 ± $4.874*10^{-03}$ cm/s with a COV of 1.46%. In the lateral direction the mean stage sped was 0.324 ± $1.221*10^{-02}$ cm/s with a COV of 3.78%. For the vertical translation the mean stage speed was 0.334 ± $8.544*10^{-03}$ cm/s with a COV of 2.56%. The maximum speed difference between the different directions was 0.051 cm/s. The results of the stage speed show that the stage moves between CPs with similar speeds revealed by the calculated COV values, which demonstrates the stability of the stage during a treatment based on CPs.

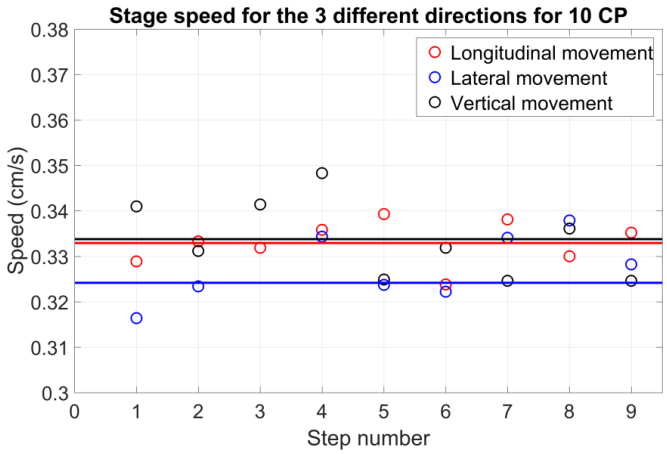


**Figure 31 –** Measured stage speed in cm/s per step for the 3 different directions for 10CP. The horizontal lines represent the mean stage speed value for each direction.

The total longitudinal stage translation for three different combinations of stage translation distances and irradiation times are shown in figure 32 a). The first combination was a translation of 2 cm over a period of 60 seconds. The second combination was a translation of 2 cm over a

period of 120 seconds. The third combinations was a translation of 3 cm over a period of 120 seconds. The horizontal lines represent the mean total stage translation for different number of CPs and for each combination. The mean total stage translation for the first combination was 1.945 ± 2.295*10$^{-03}$ cm with a COV of 0.12%, for the second combination was 1.949 ± 3.848*10$^{-03}$ cm with a COV of 0.20% and for the third combination was 2.931 ± 4.077*10$^{-03}$ cm with a COV of 0.14%. Figure 32 b) shows the total stage translation error per number of CPs for the three different combinations and the lines represent the mean error of the stage translation. The maximum mean error of 2.7% was observed for a translation of 2 cm over an irradiation period of 60 seconds. The total stage translation error for all cases varied between 2.1% and 2.9%. The low COV values and the stage movement errors below 3% over all the three combinations indicate that the stage moves in the same way regardless the number of CPs used, the stage translation distance and irradiation time.

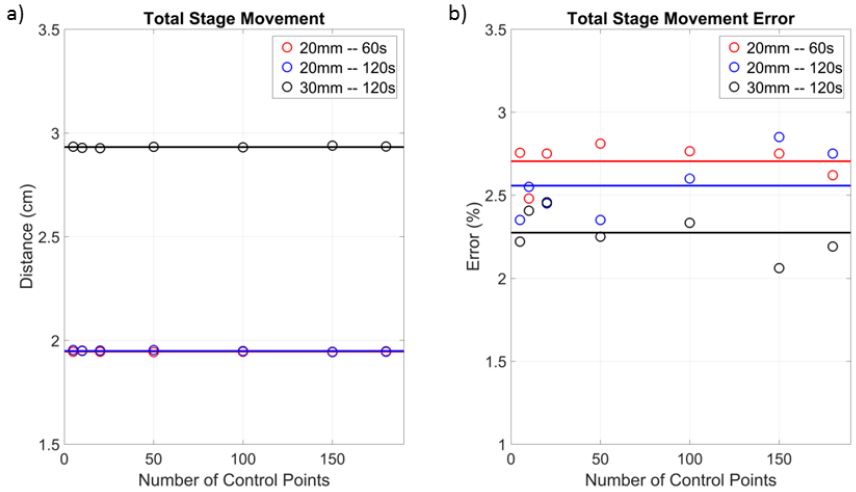


**Figure 32 –** a) Total measured stage translation in the longitudinal direction for different number of CPs and for different stage translation distances and irradiation times. The lines represent the mean total stage translation for the different combinations. b) Mean total stage translation error for the different considered CPs for the 3 different combinations. The horizontal lines represent the mean stage translation error for the different combinations.

The stage speed in the longitudinal direction for the three different combinations for 10 CPs is presented in Figure 33. The lines represent the mean stage speed for the different combinations. For the first combination, the mean stage translation speed was 0.332 ± 7.19*10$^{-03}$ cm/s with a COV of 2.17%. For the second combination the mean stage speed was 0.324 ± 1.221*10$^{-02}$ cm/s with a COV of 3.77%. For the third combination the mean stage speed was 0.406 ± 3.965*10$^{-03}$ cm/s with a COV of 2.28%. The maximum speed difference between the different translation combinations was 0.026 cm/s. The low COV values indicate that the stage moves similarly between CPs regardless the combination of stage translation distance and irradiation time used.

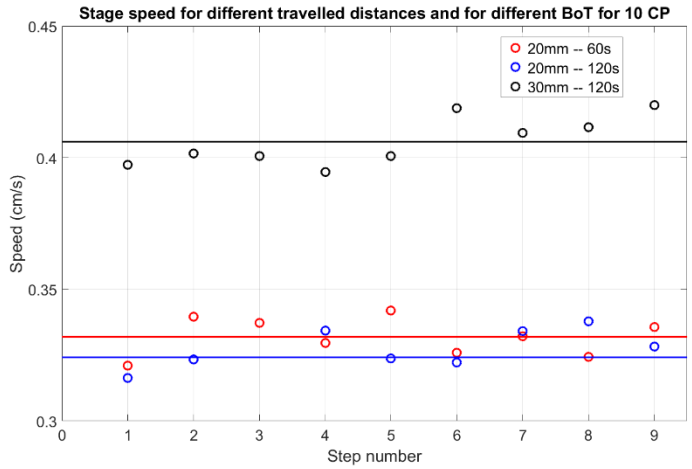


**Figure 33 -** Measured stage speed in cm/s per step in the longitudinal direction for different number of CPs and for different stage translations and irradiation times for 10CP. The horizontal lines represent the mean stage speed value for the different combinations.

## 4.2. Homogeneous dose distributions

### 4.2.1. Required distance between CPs

The standard deviation (std) of regions of interest for dose distributions delivered using different numbers of CPs for three different circular fields are shown in figure 34. To have a reasonable control of the treatment outcome, the relative standard deviation of the mean dose in the target volume should be less than 5% and, if possible, as small as 3% (Brahme, 1984). Table 3 shows the distances between CPs for a 2 mm, 5 mm and 10 mm circular fields to achieve a dose distribution COV of 3% and 5%.

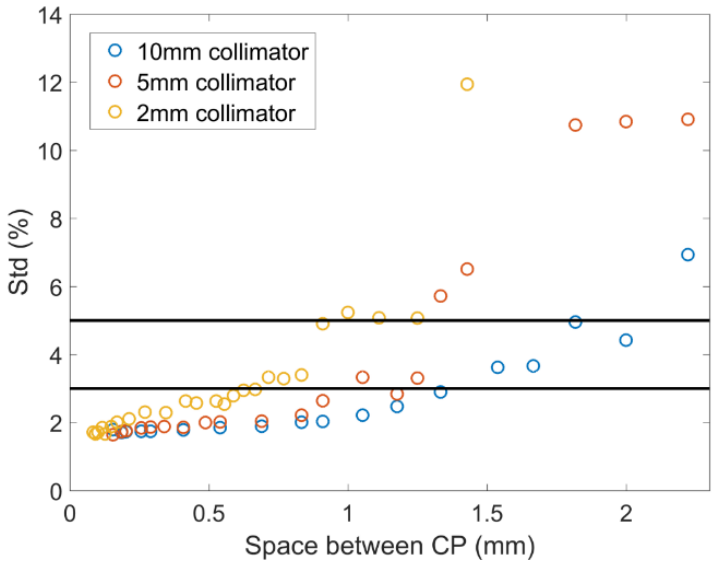


**Figure 34 –** Standard deviation of the dose distribution as function of the distance between CPs for 3 different circular fields. The black lines represent a standard deviation of 3% and 5%.

**Table 3 –** Required distance between CPs for 3 different circular fields and for a std in the region of interest of 3% and 5%.

| | Required distance between CPs' (mm) | | |
|---|---|---|---|
| **std (%)** | **2 mm beams** | **5 mm beam** | **10 mm beam** |
| 3 | 0.67 mm | 1.19 mm | 1.30 mm |
| 5 | 1.12 mm | 1.32 mm | 1.81 mm |

### 4.2.2. Evaluation of dose distribution during irradiation

#### 4.2.2.1. Stage translation & Stationary gantry

The gamma analyses between dose distributions for the stage translation in the longitudinal and lateral direction for the same number of CPs are presented in Figure 35. The gamma criteria used for the comparison were a dose difference of 3% and a distance to agreement of 0.5 mm. The highest gamma fail rate was observed for 20CP. The low gamma fail rate values indicate a similar dose distribution for the stage translation in the longitudinal and lateral direction, meaning that the stage moves similarly in both directions.

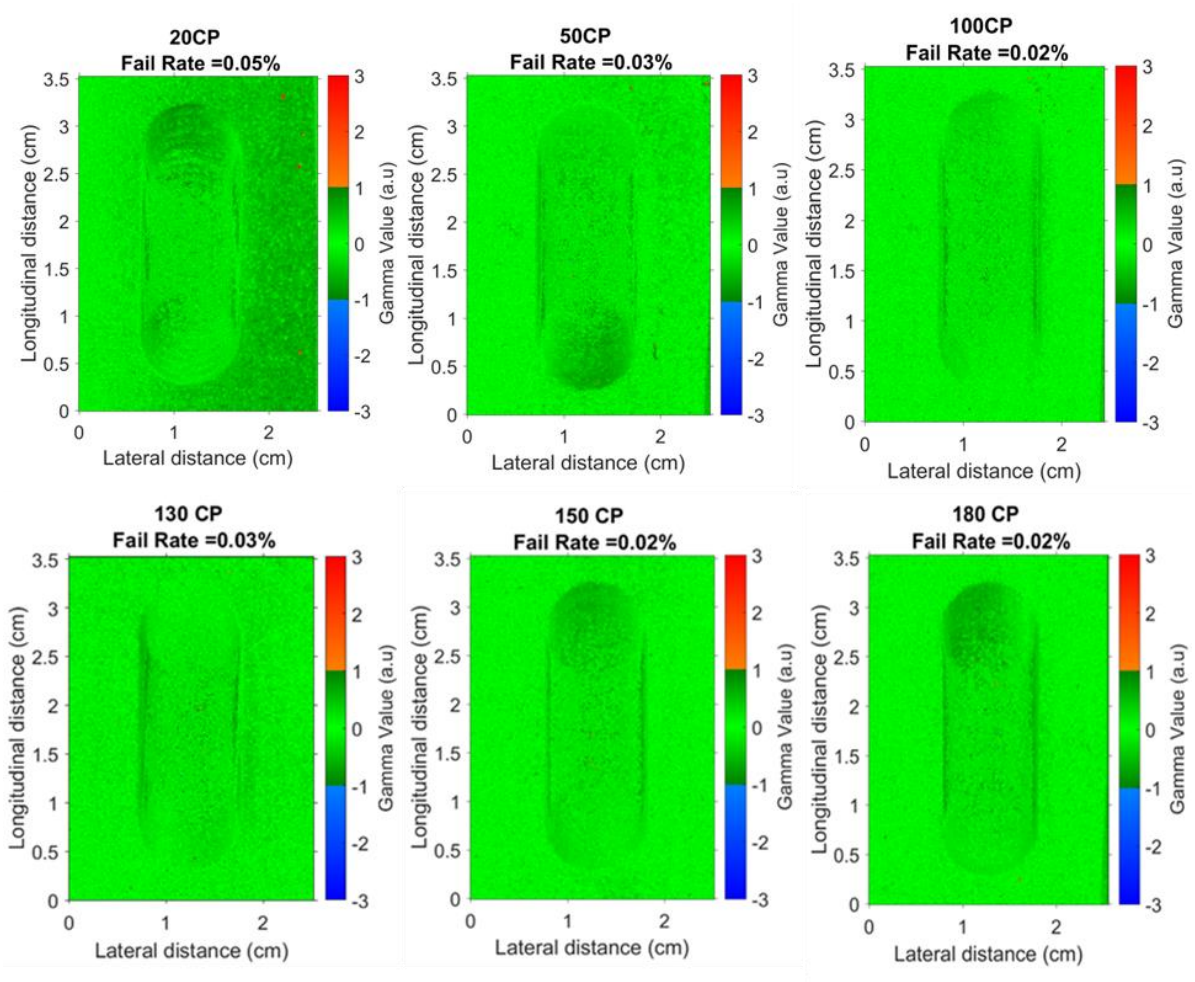


**Figure 35 –** Gamma analyses of measured dose distribution with EBT3 films between the stage translation in the longitudinal direction and lateral direction for 6 different numbers of CPs. For both directions the total stage translation was set to 2 cm, the irradiation time was 120 seconds and a 10 mm circular field was used. The gamma criteria used for the comparison were a dose difference of 3% and a distance to agreement of 0.5 mm.

Figures 36, 37, 38 and 39 present the measured and the simulated dose distribution for 20, 50, 100 and 130 CPs, respectively, for a longitudinal stage translation of 2 cm over an irradiation period of 120 seconds. The gamma analyses are also presented for the different numbers of CPs. The gamma criteria used for the comparison were a dose difference of 3% and a distance to agreement of 0.5 mm. The highest gamma fail rate was observed for 20CPs. For the rest of the cases the gamma fail rate was zero, indicating a high agreement between the measurements and the simulations.

20 CPs - Longitudinal translation

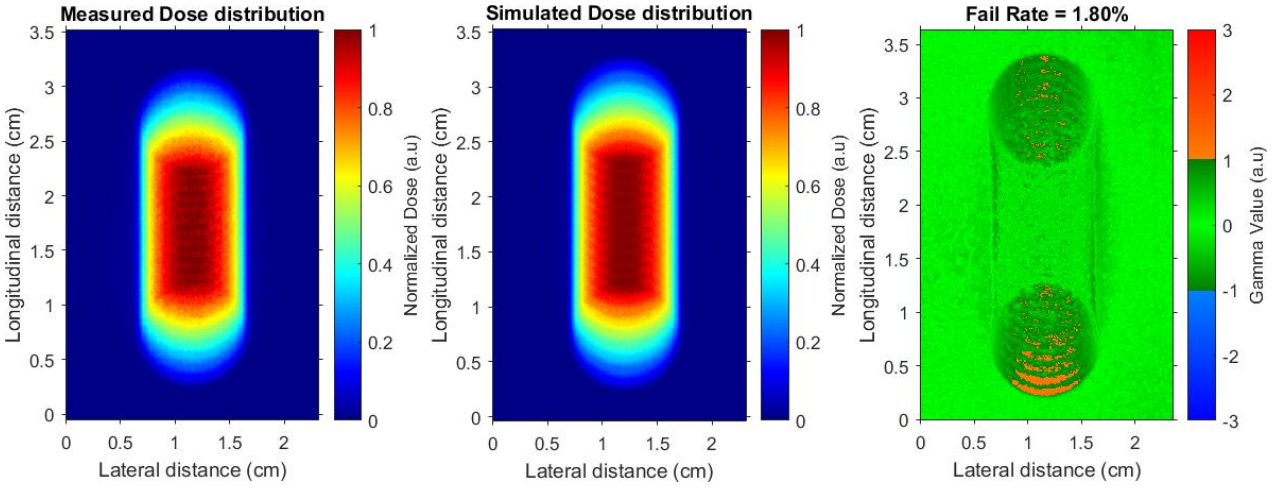


**Figure 36 –** Representation of the dose distribution measured with an EBT3 film and the simulated dose distribution as simulated on SmART-Plan for 20 CP and a total longitudinal stage translation of 2 cm over an irradiation period of 120 seconds. A circular field with a diameter of 10 mm was used for collimation. The gamma analyses is also presented. The gamma criteria used for the comparison were a dose difference of 3% and a distance to agreement of 0.5 mm.

50 CPs - Longitudinal translation

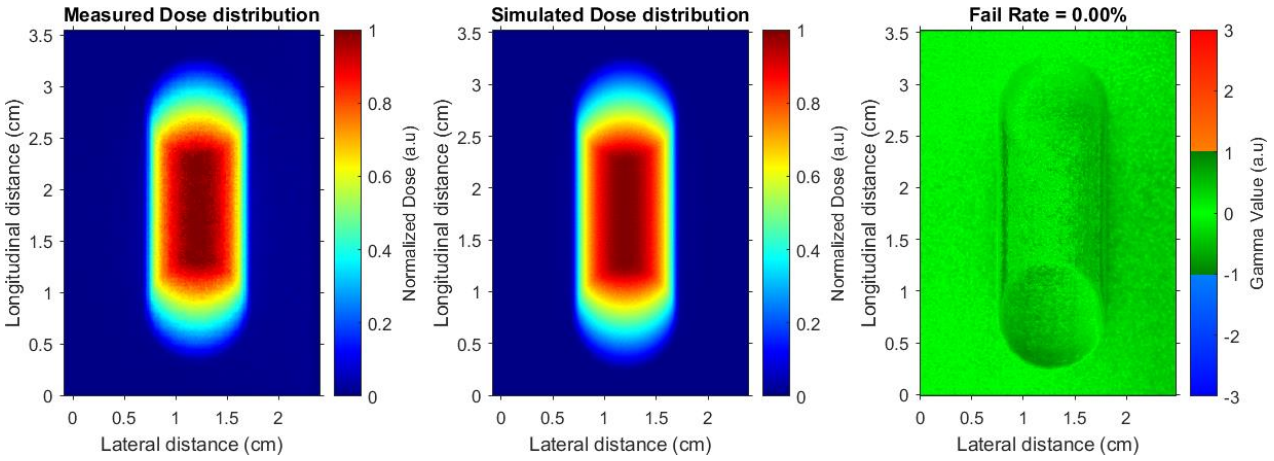


**Figure 37 -** Representation of the dose distribution measured with an EBT3 film and the simulated dose distribution as simulated on SmART-Plan for 50 CP and a total longitudinal stage translation of 2 cm over an irradiation period of 120 seconds. A circular field with a diameter of 10 mm was used for collimation. The gamma analyses is also presented. The gamma criteria used for the comparison were a dose difference of 3% and a distance to agreement of 0.5 mm.

100 CPs - Longitudinal translation

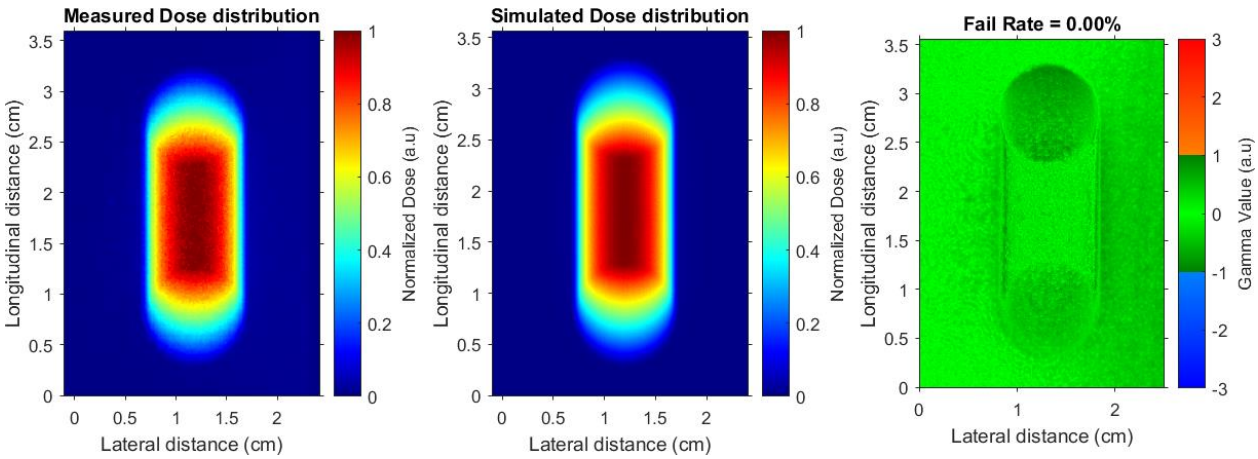


**Figure 38 -** Representation of the dose distribution measured with an EBT3 film and the simulated dose distribution as simulated on SmART-Plan for 100 CP and a total longitudinal stage translation of 2 cm over an irradiation period of 120 seconds. A circular field with a diameter of 10 mm was used for collimation. The gamma analyses is also presented. The gamma criteria used for the comparison were a dose difference of 3% and a distance to agreement of 0.5 mm.

130 CPs - Longitudinal translation

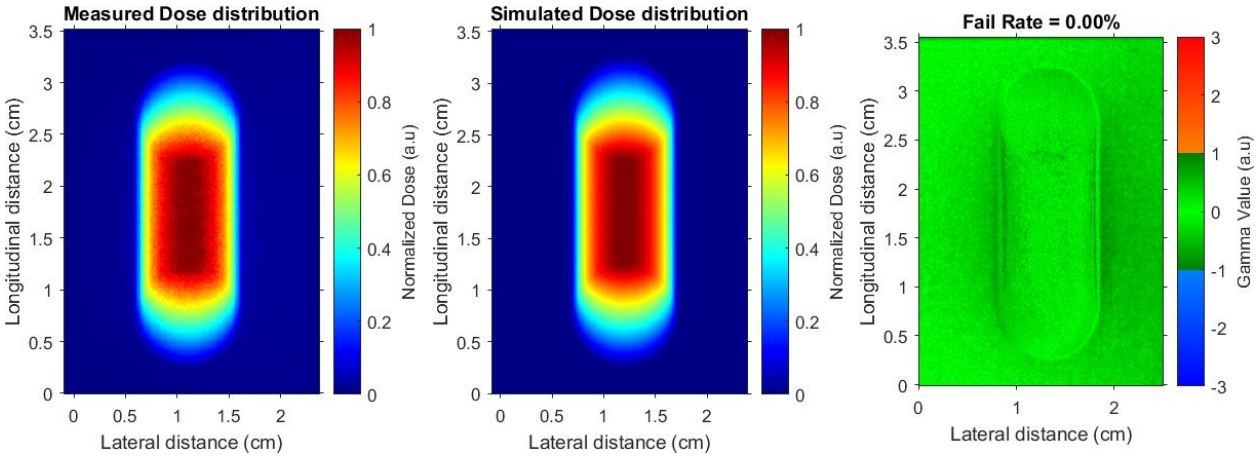


**Figure 39 -** Representation of the dose distribution measured with an EBT3 film and the simulated dose distribution as simulated on SmART-Plan for 130 CP and a total longitudinal stage translation of 2 cm over an irradiation period of 120 seconds. A circular field with a diameter of 10 mm was used for collimation. The gamma analyses is also presented. The gamma criteria used for the comparison were a dose difference of 3% and a distance to agreement of 0.5 mm.

Resulting dose profiles for the measured and simulated dose distributions for different numbers of CPs are presented in Figure 40. Dose profile lines were calculated along the longitudinal direction, as it can be observed on the dose distribution image present in Figure 40. This figure shows a good agreement between the measured and the simulated dose profiles for all cases.

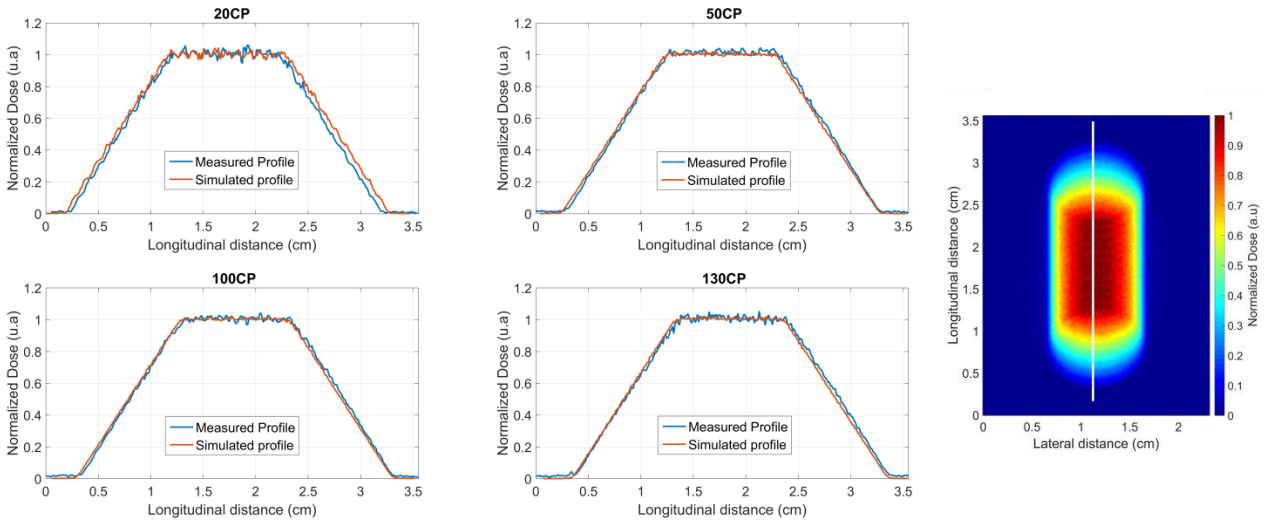


**Figure 40 –** Measured and simulated longitudinal dose profiles for 20, 50, 100 and 130 CPs for a total longitudinal stage translation of 2cm over an irradiation period of 120s. The dose profile line for the measured dose profile for 20 CPs is represented in white.

### 4.2.2.2. Stage translation & Gantry rotation

Figure 41, 42 and 43 show the measured and the simulated dose distributions for 25, 50 and 100 CPs, respectively, and the gamma analyses between both dose distributions, for a longitudinal stage translation of 2 cm and a simultaneous full gantry arc revolution. Both the stage translation and full gantry rotation were performed using the same number of CPs. The gamma criteria used for the comparison were a dose difference of 5% and a distance to agreement of 1.0 mm. The fail rates are also shown for each CP comparison. The highest gamma fail rate was observed for 25 CPs. For the rest of the cases the gamma fail rate was zero, meaning that there is not a single pixel failing in the gamma analyses. These results reveal a high agreement between the measurements and the simulations.

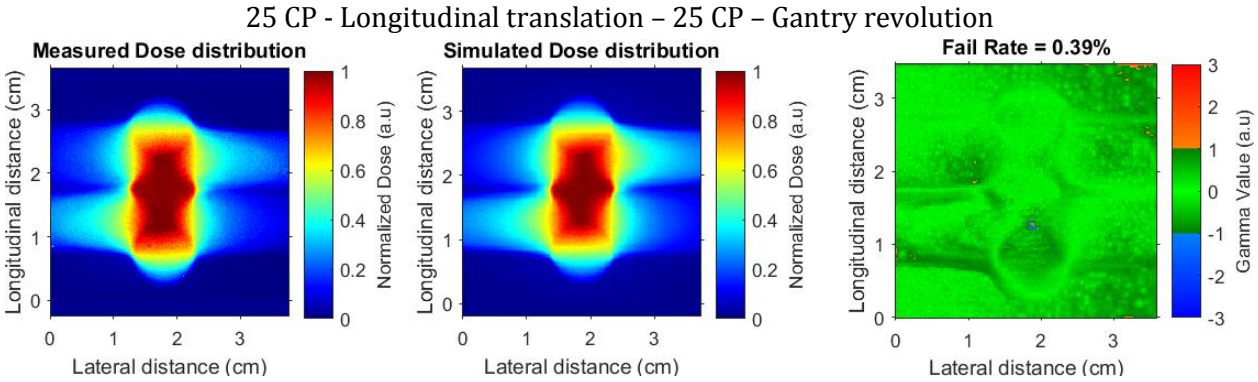


**Figure 41 -** Measured dose distribution with EBT3 film and the simulated dose distribution using SmART-Plan for 25 CPs for a total longitudinal stage translation of 2 cm and a full gantry arc revolution over an irradiation period of 200 seconds. The gamma criteria used for the comparison was a dose difference of 5% and a distance to agreement of 1.0 mm.

50 CP - Longitudinal translation – 50 CP – Gantry revolution

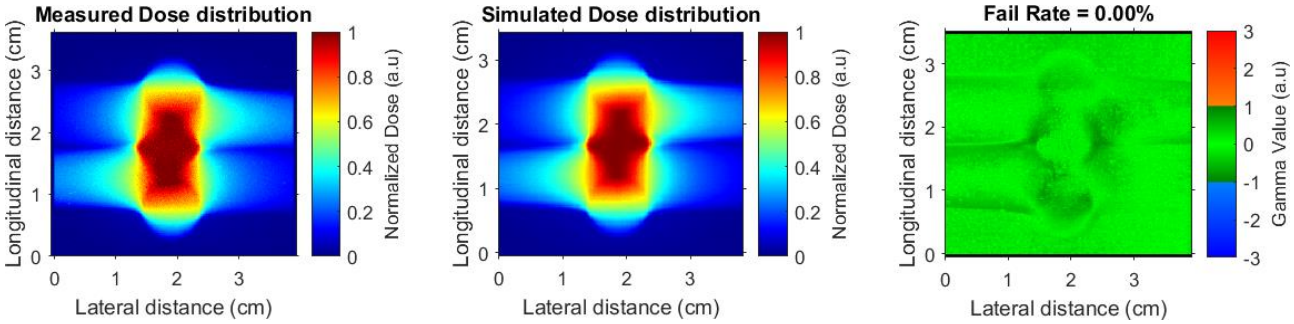


**Figure 42 -** Measured dose distribution with EBT3 film and the simulated dose distribution using SmART-Plan for 50 CPs for a total longitudinal stage translation of 2 cm and a full gantry arc revolution over an irradiation period of 200 seconds. The gamma criteria used for the comparison was a dose difference of 5% and a distance to agreement of 1.0 mm.

100 CP - Longitudinal translation – 100 CP – Gantry revolution

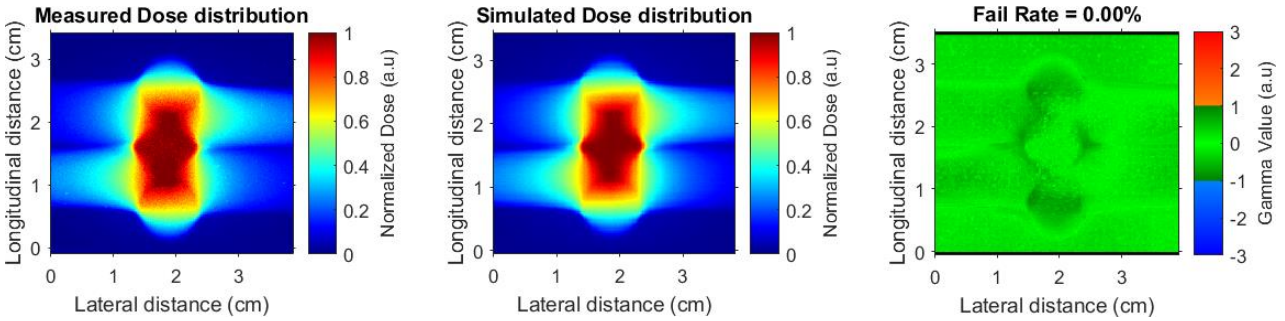


**Figure 43 -** Measured dose distribution with EBT3 film and the simulated dose distribution using SmART-Plan for 100 CPs for a total longitudinal stage translation of 2 cm and a full gantry arc revolution over an irradiation priod of 200 seconds. The gamma criteria used for the comparison was a dose difference of 5% and a distance to agreement of 1.0 mm.

## 4.3. Need of additional spatial degrees of freedom in small animal radiotherapy

### 4.3.1. Mouse Glioblastoma case

Different treatment plans with different beam configurations were simulated for a mouse glioblastoma case and are presented in figure 44. Two volumes of interest were delineated, the normal brain (V = 320 $mm^3$) and the brain tumor (V = 4 $mm^3$). Figure 45 shows the DVHs for the glioblastoma and for the normal brain for the three simulated treatment cases. When analyzing the brain DVH for the different cases, the second case delivers a higher dose to the normal tissue brain. When comparing the brain DVH between case 1 (standard treatment) and case 3, there is no visible difference. The DV metrics for the brain for the three cases are shown in table 4. Case 2 presents a higher mean dose delivered to the normal brain, but case 3 presents a higher $D_{1\%}$, a higher maximum dose ($D_{max}$) and a higher $D_{5\%}$.

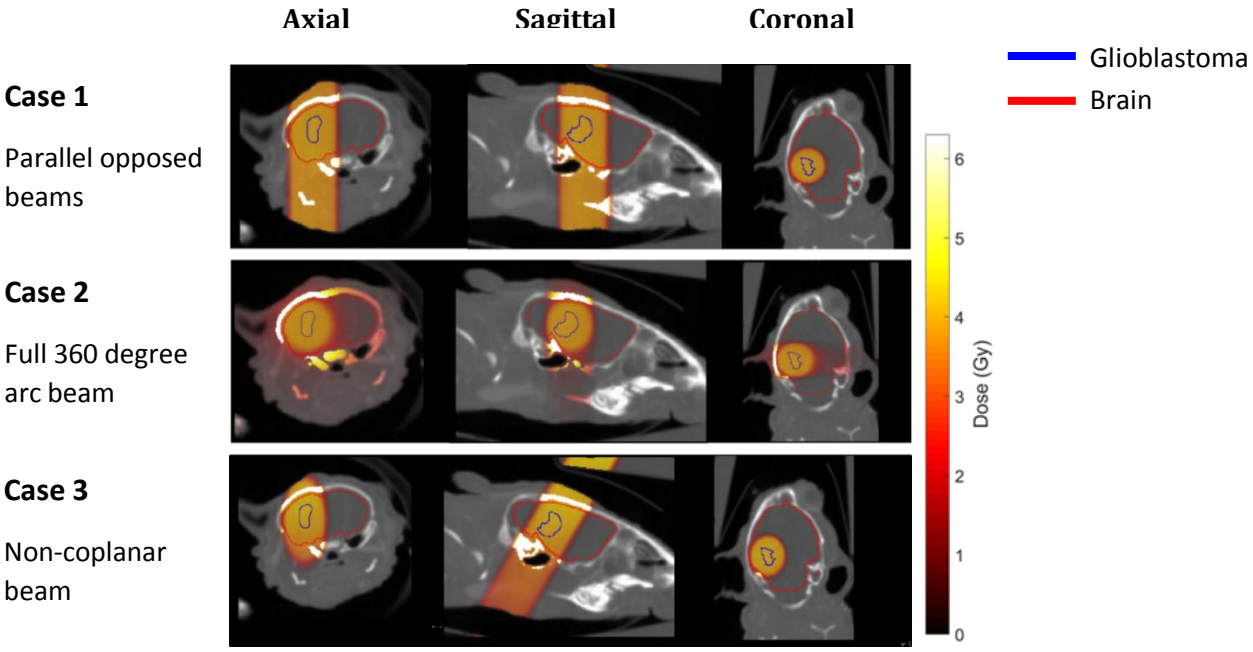


**Figure 44 –** Different views of the dose distribution for 3 treatments plans for a mouse brain tumor case. The prescription dose to the tumor was 4Gy. For each case, the first dose distribution image (left) represents a slice in the axial plane, the second dose distribution image (middle) represents a slice in the sagittal plane and the third dose distribution image (right) represents a slice in the coronal plane.

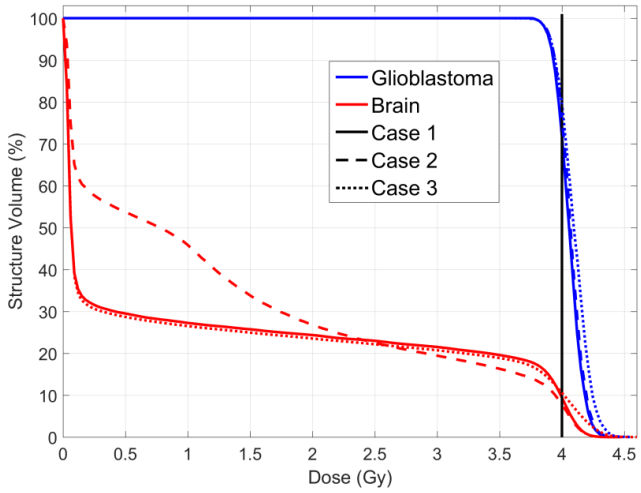


**Figure 45 –** DVHs obtained for glioblastoma and normal brain for the 3 considered treatment cases represented by different lines. The DVHs for the different cases were scaled to the same V95% of the tumor. The vertical black solid line indicates the prescription dose to the tumor, 4 Gy.

**Table 4 –** DV metrics of the normal brain tissue for the 3 treatment cases.

| | Brain | | |
|---|---|---|---|
| **D (Gy)** | **Case 1** | **Case 2** | **Case 3** |
| $\mathbf{D_{mean}}$ | 1.01 | 1.30 | 0.99 |
| $\mathbf{D_{5\%}}$ | 4.07 | 4.06 | 4.16 |
| $\mathbf{D_{max}}$ | 4.46 | 4.49 | 4.67 |
| $\mathbf{D_{1\%}}$ | 4.18 | 4.18 | 4.33 |

### 4.3.2. Mouse Right Lung tumor case

Different treatment cases for a mouse lung tumor were simulated. The respective overview is shown in Figure 46. Seven different structures were considered and they can be visualized in figure 46, delineated with different colors. The lung tumor (V=30 $mm^3$) was located in the right lung (V=220 $mm^3$). Figure 47 shows the DVHs for the tumor and for the 6 OARs for the 3 treatment cases. When analyzing the OAR DVHs for the different cases, it must be highlighted that case 3 is the one delivering more dose to the heart and stomach. The treatment plan from case 2 is the only treatment plan delivering zero dose to the right lung. This treatment plan also delivers less dose to the left lung but delivers more dose to the liver. Different DV metrics for the 6 OAR for the 3 cases are shown in Figure 47. The biggest differences on the DV metrics are present for case 3, where there is no dose delivered to the left lung and there is a higher dose delivered to the liver.

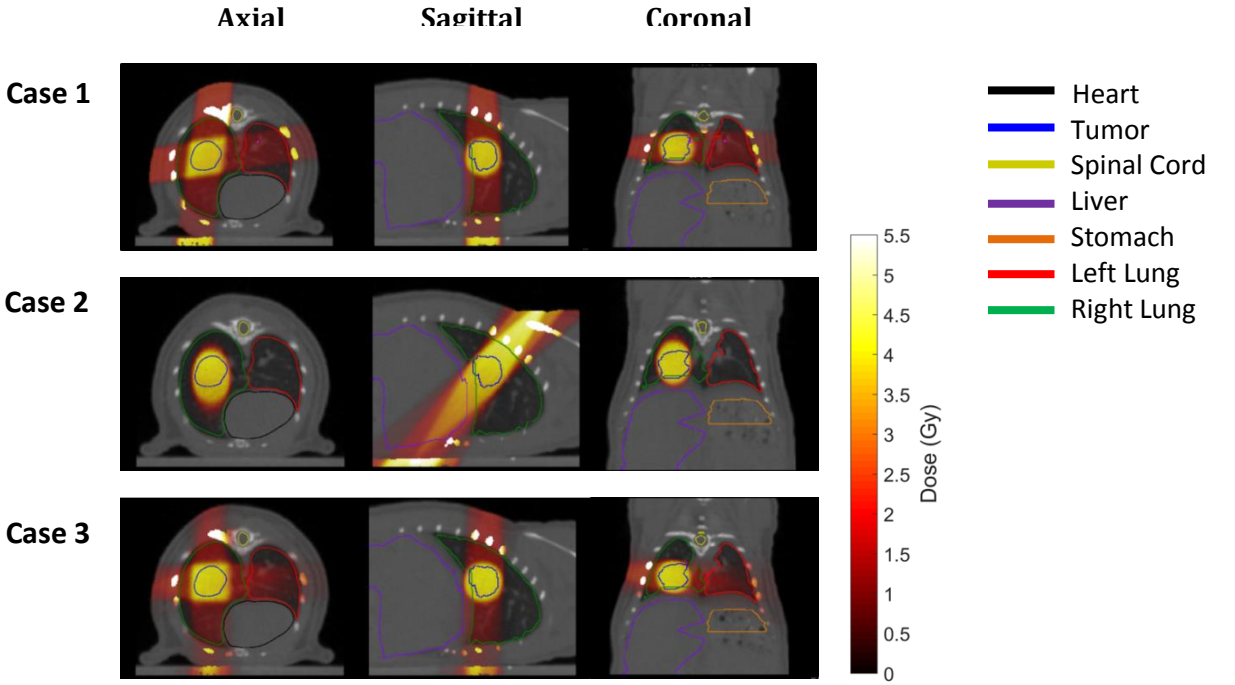


**Figure 46 –** Different views of the dose distribution for 3 treatments plans for a lung tumor case with a prescription dose of 4 Gy. The first dose distribution image represents a slice in the axial plane, the second dose distribution image represents a slice in the sagittal plane and the third dose distribution image represents a slice in the coronal plane.

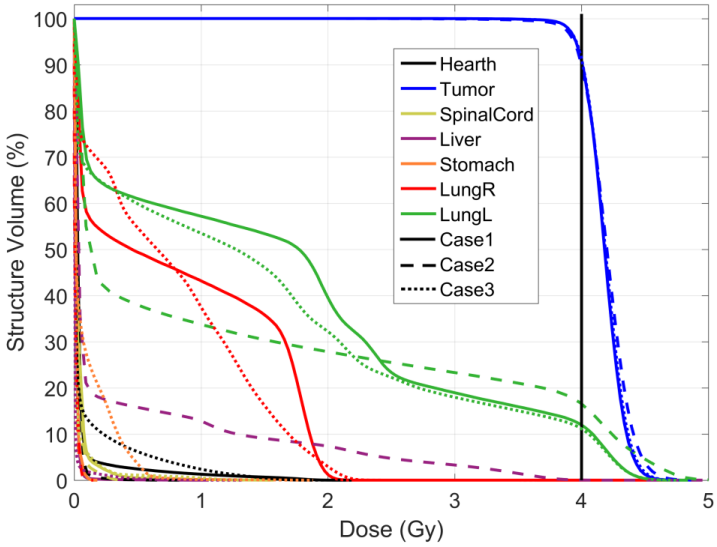


**Figure 47 -** DVHs obtained for the lung tumor and for the different considered OARs, for the 3 considered treatment cases. The DVHs for the different cases were scaled to the same V95% of the tumor. The vertical black solid line indicates the prescription dose to the tumor, 4 Gy.

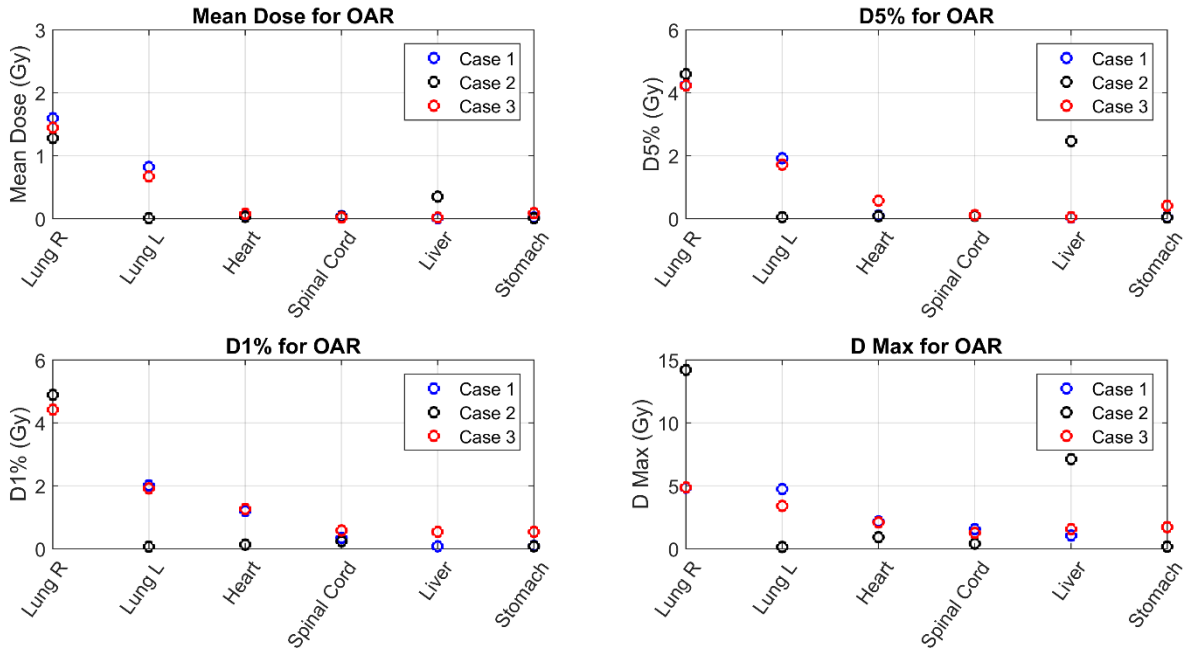


**Figure 48 –** DH metrics of the OARs obtained for the lung tumor, for the 3 treatment cases.

## 4.4. Treatment based on stage translation

A treatment case based on different stage positions was simulated for a mouse lung tumor case and the resulting dose distribution is presented in Figure 49 as case 2. In Figure 49 it is also represented another case, case 1, based on a single stage position with a similar beam configuration of case 2 for comparison. Figure 49 shows similar dose distributions for both cases. Looking to the coronal view is visible some degree of conformity of the dose to the tumor when a treatment based on a stage translation is used. The DVHs of the tumor and the 6 OARs for the 2 treatment cases are presented in Figure 50. Figure 50 shows a higher delivered dose to the tumor,

right lung and heart when the treatment is based on multiple stage positions. For the remaining OAR the DVHs are similar.

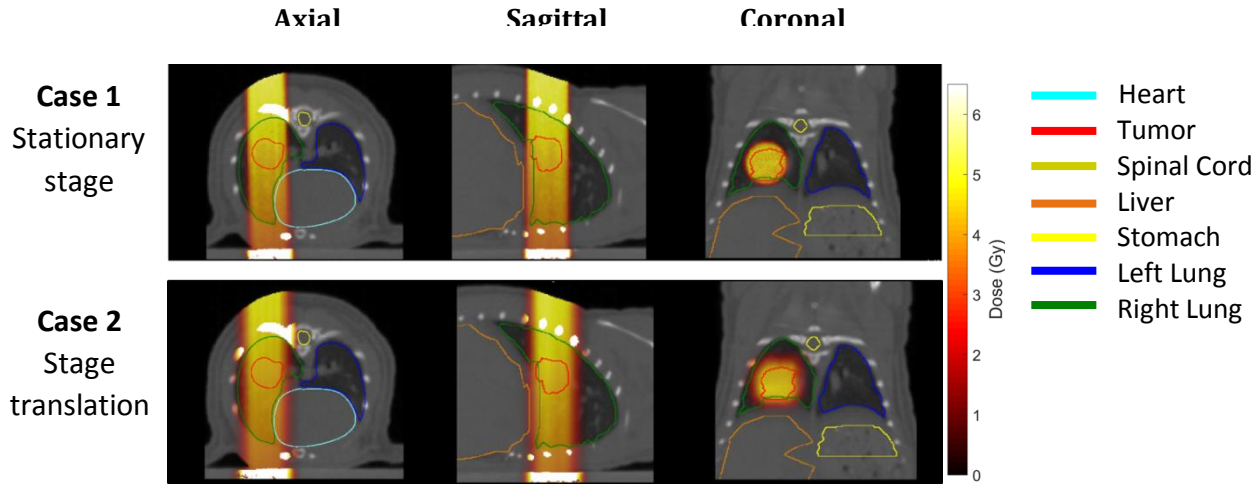


**Figure 49 -** Different views of the dose distribution for 2 different treatments plans, the first one based on a single stage position and the other based on multiple stage positions, for a lung tumor case with a prescription dose of 4 Gy. The first dose distribution image represents a slice in the axial plane, the second dose distribution image represents a slice in the sagittal plane and the third dose distribution image represents a slice in the coronal plane.

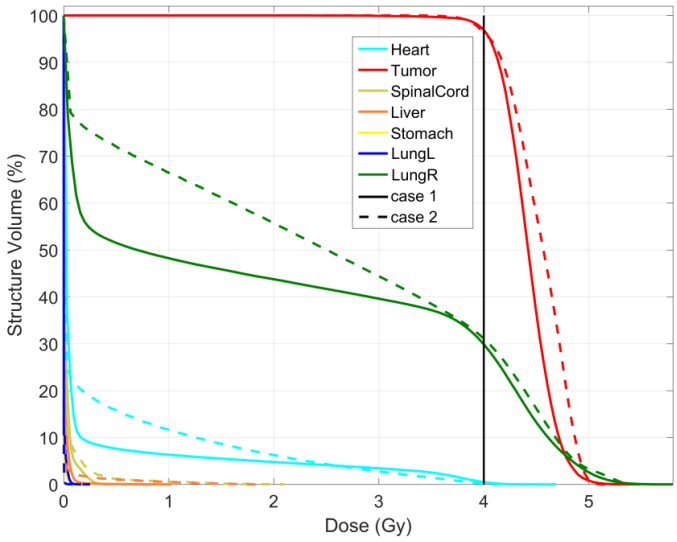


**Figure 50 -** DVHs obtained for the lung tumor case and for the different considered OARs, for 2 different treatments, the first one based on a single stage position and the other based on multiple stage positions. The DVHs for the different cases were scaled to the same V95% of the tumor. The vertical black solid line indicates the prescription dose to the tumor, 4 Gy.

# 5. DISCUSSION

The feasibility of delivering complex dose distributions through stage and gantry movement was investigated in this thesis. The delivery of complex dose distributions is accomplished by treatment protocols based on different numbers of CPs. The stage translation was investigated and according to the results regardless of the stage translation direction the movement is not dependent on the number of CPs used. The results also show a stage movement between CPs with similar speeds, which demonstrate the stability of the stage translation during a treatment based on CPs. The stage translation is neither dependent of the irradiation time nor the stage translation distance. The high agreement between the simulations and measurements indicate that the stage reproduces in the correct way what is specified in the protocols. Initially, during the first experiments, was discovered that the delivered dose was increasing with the number of CPs. This increase was later explained by the increase of the irradiation period when the number of CPs also increases (Appendix E). Once the error was found, an update was performed to the small animal platform and the error was fixed. The results presented here, in this thesis, are relative to the small animal platform after the update.

The need of spatial degrees of freedom in small animal radiotherapy, where treatments based on beams delivered from multiple directions instead of beams only delivered from angles allowed by the gantry rotation for the mouse glioblastoma case, showed that there is not a significant difference between a treatment based on a standard treatment plan used in current pre-clinical practice (case 1) and a treatment based on a beam delivered from an angle not allowed by the gantry (case 3). The high dose delivered to the normal brain seen for case 2, is due to the use of a full 360 arc beam which irradiates a higher volume of the normal brain. Based on the mouse glioblastoma treatment case the delivery of beams from additional angles do not improve the treatment. Nevertheless, is important to be aware that this is a simple case where just two structures were considered. Regarding the mouse right lung tumor case there is a clear improvement of the DVHs of the OARs when treatments based on beams delivered from directions not allowed by the gantry (non co-planar beams) are used. The main difference is seen for the dose delivered to the left lung since with the correct beam geometry this structure can be completely avoided. This thesis shows a case where additional degrees of freedom may not improve the treatment but in contrast a treatment improvement is also shown when beams delivered from different directions are used. In this way, more cases with different types of cancer and cancer geometries need to be investigated in order to better understand when the use of additional degrees of freedom is translated in a real improvement of the treatment plans.

The mouse lung tumor treatment simulation based on stage translation showed higher delivered doses to some structures when compared with a treatment based on a single stage position. This can be explained by dose overlapping on some stage positions which creates hot spots increasing the dose on those structures. The case studied here was based on 316 different stage positions and trying to simulate a treatment with such a high number of different stage positions is time and memory consuming and is important to keep in mind that the animal is under anesthesia during the entire process, which includes the time to perform the simulations. Another important aspect is the delivery of the treatment itself, which if it was based on so many stage positions the irradiation would be nearly impossible. In this way it is extremely important to create a beam optimizer not only capable of beam optimization but also capable of reducing the number of stage positions.

# 6. CONCLUSION

In this thesis complex dose distributions were delivered with treatments based on stage and gantry movement. This was done through the use of CP based treatment plans for the first time in small animal radiotherapy. The stage positioning and translation during irradiation was proven to be accurate and reliable and the irradiator can handle large number of CPs without problems. The study of the dose distributions showed a high agreement between the film measurements and simulations. According to what was investigated in this thesis, it is safe to say that SmART platform is capable of delivering complex dose distributions based on stage and gantry movement.

# 7. FUTURE PERSPECTIVES

Hardware for precision image-guided small animal radiotherapy is evolving rapidly and catching up with clinical irradiation capabilities. These improvements of pre-clinical radiotherapy research platforms require equally improving software and algorithms to plan, evaluate and control the hardware. However, since treatment goals and restrictions in pre-clinical research can be vastly different from the clinical setting, it is not necessarily the case that pre-clinical research platforms require or need to pursue the same development path their clinical counterparts have gone through. This can be applied, for example, to the beam-shaping multileaf collimator on an accelerator used in clinical practice, which is essential in radiotherapy, but would be very hard to miniaturize for small animal radiotherapy platforms.

Data indicates that treatments capable of delivering beams from additional directions may provide benefits over standard treatments, if the correct beam geometry and configuration are used. Nevertheless more mice tumor cases with different tumors locations, sizes and geometries need to be investigated. To better and faster investigate this issue, a beam optimizer capable of beam weights optimization and of automatically choosing the optimum beams combination and geometry is desirable.

With a gantry and stage capable of rotating 360 degrees the target can be irradiated from any desired direction and angle, which brings a new set of possibilities. In this way, it is important to outline some priorities and define what are the main OAR to avoid and also define dose constraints for animal studies. Furthermore, it is also important to understand and prioritize, for each individual case, what is more important: trying to avoid some OAR or irradiate the tumor with the maximum possible dose accuracy. All of these are questions that need to be addressed and that are very important to improve radiotherapy studies in small animals. Along with this, better imaging techniques that enable better tissue segmentation are crucial to help to answer all these questions. Recently, some advances have been made in this particular field with the development of dual Energy CT in small animal radiotherapy (Schyns et al., 2016).

In comparison with a treatment based on a single stage position, the simulations of treatments based on multiple stage positions showed high delivered doses to some structures. A possible way to compensate for this, could be through a treatment plan optimizer capable of delivering automatically homogeneous dose distributions avoiding the creation of hot spots and reduce as much as possible the number of different required stage position. It would also be interesting to investigate the possibility of achieving treatments with similar outcomes/qualities when treatments based on stage translation and gantry rotation are compared with treatment based on

stage and rotation, which it is not possible yet. Regardless the preferable chosen technique in both ways to maximize the benefits of the capabilities of image-guided small animal radiotherapy platforms, treatment planning automation and inversion is required to deliver more complex dose distributions.

With gantry and stage movement all geometric degrees of freedom can be achieved. In small animal radiotherapy, the adjustment of the voltage potential of the X-Ray tube is also possible, which allows the altering of the maximum photon energy. By lowering the photon energy, the dose gradient in the animal will change compared to the standard photon energy. Hence, distant organs at risk are more likely to be spared. It would also be interesting to understand if treatment plans based on lower kV photon energies could improve the treatment.

It is also important to have in mind that, with stage and gantry movement, it is possible to deliver heterogeneous dose distributions, making dose painting studies a possible next step in small animal radiotherapy. Heterogeneous doses can also be achieved by changing photon's energy during treatment. In this way, treatments with a dynamic change in photon's energy could be a different/complementary approach to the gantry and stage movement.

As final words, along with the development and improvement of small animal radiotherapy platforms and small animal cancer models, has come the growth in fundamental knowledge and greater translational insight, that should further extend our still incomplete genetic and molecular understanding of cancer. These new knowledges can later be used to ensure better methods for cancer detection, diagnosis and treatment. Currently, research and introduction of new drugs and treatments into clinical practice in terms of safety and efficacy is still far away from a point where research and validation should preferably be done without the use of small animals.

# 8. REFERENCES


Balvert, M. (2015). A framework for inverse planning of beam-on times for 3D small animal radiotherapy using interactive multi-objective optimisation. *Physics in Medicine and Biology*. 60: 5681-5698.

Bartling, S. H., *et al* (2008). Gating in small-animal cardio-thoracic CT. *Methods.* 50: 42-49.

Bartling, S. H., *et al* (2010). Intrinsic respiratory gating in small-animal CT. *European Radiology.* 18: 1375–1384.

Beekman, F. J., & Vastenhouw, B. (2004). Design and simulation of a high-resolution stationary. *Physics in medicine and biology.* 49: 4579–4592.

Bentzen SM, Gregoire V. (2011). Molecular imaging-based dose painting: a novel paradigm for radiation therapy prescription. *Seminars in Radiation Oncology*. 21: 101-110.

Bolcaen, J. (2014). MRI-guided 3D conformal arc micro-irradiation of a F98 glioblastoma rat model using the Small Animal Radiation Research Platform (SARRP). *Journal of Neural Oncology*. 120: 257-266.

Bouchard, H. *et al* (2009). On the characterization and uncertainty analysis of radiochromic film dosimetry. *Medical Physics*. 36: 1931:1946.

Brahme, A. (1984). Dosimetric Precision Requirements in Radiation Therapy. *Acta Radiologica: Oncology*. 23: 379-391.

Butterworth, K. T. *et al* (2014). Small animal image-guided radiotherapy:status, considerations and potencial for translational impact. *The British Journal of Radiology*. 88: 20140634.

Cho, N. B., & Kazanzides, P. (2012). A Treatment Planning System for the Small Animal Radiation Research Platform (SARRP) based on 3D Slicer. *MIDAS Journal*.

Cho, N. B., Wong, J., & Kazanzides, P. (2014). Dose Painting with a Variable Collimator for the Small Animal Radiation Research Platform (SARRP). *MIDAS Journal*.

CRUK (2015). Radiotherapy. Retrieved 11-20-2015, from Cancer Research UK: http://www.cancerresearchuk.org/science/research/who-and-what-we-fund/topic/radiotherapy/

Depuydt, T. *et al* (2001). A quantitative evaluation of IMRT dose distributions: refinement and clinical assessment of the gamma evaluation. *Radiotherapy and Oncology*. 62: 309–319

Freeman, T. (2014-4-10). Dose painting: checking the uncertainties. Retrieved 12-4-2015, from medicalphysicsweb: http://medicalphysicsweb.org/cws/article/research/56879.

Granton, P. V. (2012). A combined dose calculation and verification method for a small animal precision irradiator based on onboard imaging. *Medical Physics*. 39: 4155-4166.

Granton, P. V. (2014). A Longitudinal Evaluation of Partial Lung Irradiation in Mice by Using a Dedicated Image-Guided Small Animal Irradiator. *International Journal of Radiation Oncology, Biology and Physics*. 20: 696-704.

Hoof, S. v. (2012). Triple Channel Film Dosimetry and its Application to Small Animal Rdiation Therapy. Master Thesis. Department of Biomedical Engineering, Eindhoven University of Technology.

Hoof, S. J. *et al* (2012). Evaluation of a novel triple-channel radiochromic film analysis procedure using EBT2. *Physics in Medicine and Biology*. 57: 4353–4368.

Hoof, S. J., Granton, P. V., & Verhaegen, F. (2013). Development and validation of a treatment planning system for small animal radiotherapy: SmART-Plan. *Radiotherapy and Oncology*. 109: 361-366.

Jeong, J. *et al* (2015). Adaptation, Commissioning, and Evaluation of a 3D Treatment Planning System for High-Resolution Small-Animal Irradiation. *Technology in Cancer Research & Treatment*. 1-12.

Kroon, M. (2015). A beam selection procedure based on dose calculation inaccuracies for small animal radiation therapy. Master Thesis. Tilburg School of Economics and Management Tilburg University.

Kuntz, J., *et al* (2010). Fully automated intrinsic respiratory and cardiac gating for small animal CT. *Physics in Medicine and Biology*. 55: 2069–2085.

Low, D. A. *et al* (1998). A technique for the quantitative evaluation of dose distributions. *Medical Physics*. 25: 656-661.

Lotte, S. *et al* (2016). Time-resolved versus time-integrated portal dosimetry. The role of the isocenter position in volumetric modulated arc therapy. Master Thesis. Eindhoven University of Technology.

Marchant T., & Moore, C. (2014). Monte Carlo modelling of the Small Animal Radiation Research Platform (SARRP). Retrieved 12-10-2015, from http://www.hep.man.ac.uk/u/wyatt/MPhysProjectPlanSARRP.pdf

McCarroll, R. *et al* (2015). 3D-Printed Small-Animal Immobilizer for Use in Preclinical Radiotherapy. *Journal of the American Association for Laboratory Animal Science*. 54: 545–548.

Motamura, R. *et al* (2010). Investigation of the effects of treatment planning variables in small animal radiotherapy dose distributions. *Medical physics*.37: 590-599.

NIH (2010). Radiation Therapy for Cancer. Retrieved 12-10-2015, from http://www.cancer.gov/about-cancer/treatment/types/radiation-therapy/radiation-fact-sheet

Nordström, F. (2012). Quality Assurance in Radiotherapy - Development and evaluation of new tools for improved patient safety. Lund University.

PXI - Precision X-RAY. (2012). XRad 225Cx Software User's Manual. Operating Instructions X-RAD 225Cx.

PXI - Precision X-RAY. (2015). X-RAD SmART (Small Animal RadioTherapy) IMAGE GUIDED BIOLOGICAL IRRADIATOR Technical Specifications. X-rad smart technical brochure.

Rubinstein, A., *et al* (2013). SU-D-144-03: respiratory motion management for high-precision small animal irradiation respiratory motion management for high-precision small animal irradiation. *Medical Physics*. 40: 116.

Schyns, L. *et al* (2016). Time-resolved versus time-integrated portal dosimetry: the role of an object's position with respect to the isocenter in volumetric modulated arc therapy. *Physics in Medicine and Biology*. 61: 3969-3984.

Society, A. C. (2014). The Science Behind Radiation Therapy. Atlanta, Georgia: Copyright American Cancer Society.

Stewart BW, Wild CP. (2014). Global battle against cancer won't be won with treatment alone Effective prevention measures urgently needed to prevent cancer crisis. Lyon, France: International Agency for Research on Cancer.

Stojadinovic, S. *et al* (2008). MicroRT—Small animal conformal irradiator. *Medical physics*.34: 4706-4716.

The Slicer Community, (2015). 3DSlicer. Retrieved 12-10-2015, from Wikipedia: https://en.wikipedia.org/wiki/3DSlicer.

Tillner, F., *et al* (2016). Precise image-guided irradiation of small animals: a flexible non-profit platform. *Physics in Medicine and Biology*. 61: 3084–3108.

Verhaegen, F., Granton, P., & Tryggestad, E. (2011). Small animal radiotherapy research platforms. *Physics in medicine and biology*. 56: R55-R83.

Verhaegen, F. *et al* (2014). A review of treatment planning for precision image-guided photon beam pre-clinical animal radiation studies. *Zeitschrift für Medizinische Physik*. 24: 323–334.

WCRF International. Worldwide data. Retrieved 11-20-2015, from World Cancer Research Foundation: http://www.wcrf.org/int/cancer-facts-figures/worldwide-data.

WHO. Cancer. Retrieved 11-20-2015, from World Health Organization: http://www.euro.who.int/en/health-topics/noncommunicable-diseases/cancer

Winiecki, J. *et al* (2009). The gamma evaluation method as a routine QA procedure of IMRT. *Reports of Practical Oncology and Radiotherapy*. 14:162–168.

Wong, J. *et al* (2008). High-ResolutionsSmall animal irradiator research platform with X-ray tomographic guidance capabilities. *International journal of radiation oncology, biology, physics*. 71: 1591-1599.

Workman, P *et al* (2010). Guidelines for the welfare and use of animals in cancer research. British Journal of Cancer. 102: 1555–1577.

Yahyanejad, S. (2015). An image guided small animal radiation therapy platform (SmART) to monitor glioblastoma progression and therapy response. *Radiotherapy and Oncology*.

Zhou, H. (2010). Development of micro-computed tomography-based image-guided conformal radiotherapy system for small animals. *International journal of radiation oncology, biology, physics*. 1-9.

## APPENDIX A – TREATMENT PROTOCOL

Here is presented an example of a protocol used to evaluate the stage positioning of the XRAD-225Cx device. This protocol delivers a treatment with a total stage translation of 2 cm in the longitudinal direction divided by 11 CPs.

```
[Protocol]
Name= Protocol 1
Version=1
Description= total stage translation = 2cm; direction = longitudinal; number of
control points = 10

[Beam0]
BeamNumber=1
BeamName=Beam 1
BeamDescription=Beam 1
UserInstructions=lln
BeamType=STATIC
RadiationType=PHOTON
PrimaryDosimeterUnit=MINUTE
FinalCumulativeMetersetWeight=100
BeamOnTime=120

[Beam0 - ControlPoint0]
CumulativeMetersetWeight=0.00
NominalBeamEnergy=0.010
NominalTubeCurrent=13
SpotSize=LARGE
GantryAngleIEC=0
GantryRotationDirection=NONE
TableTopVerticalPosition=0.00
TableTopLongitudinalPosition=0.00
TableTopLateralPosition=0.00

[Beam0 - ControlPoint1]
CumulativeMetersetWeight=10.00
NominalBeamEnergy=0.010
NominalTubeCurrent=13
SpotSize=LARGE
GantryAngleIEC=0
GantryRotationDirection=NONE
TableTopVerticalPosition=0.00
TableTopLongitudinalPosition=-2.00
TableTopLateralPosition=0.00

[Beam0 - ControlPoint2]
CumulativeMetersetWeight=20.00
NominalBeamEnergy=0.010
NominalTubeCurrent=13
SpotSize=LARGE
GantryAngleIEC=0
GantryRotationDirection=NONE
TableTopVerticalPosition=0.00
TableTopLongitudinalPosition=-4.00
TableTopLateralPosition=0.00

[Beam0 - ControlPoint3]
CumulativeMetersetWeight=30.00
NominalBeamEnergy=0.010
NominalTubeCurrent=13
SpotSize=LARGE
GantryAngleIEC=0
GantryRotationDirection=NONE
TableTopVerticalPosition=0.00
TableTopLongitudinalPosition=-6.00
TableTopLateralPosition=0.00
```

```
[Beam0 - ControlPoint4]
CumulativeMetersetWeight=40.00
NominalBeamEnergy=0.010
NominalTubeCurrent=13
SpotSize=LARGE
GantryAngleIEC=0
GantryRotationDirection=NONE
TableTopVerticalPosition=0.00
TableTopLongitudinalPosition=-8.00
TableTopLateralPosition=0.00

[Beam0 - ControlPoint5]
CumulativeMetersetWeight=50.00
NominalBeamEnergy=0.010
NominalTubeCurrent=13
SpotSize=LARGE
GantryAngleIEC=0
GantryRotationDirection=NONE
TableTopVerticalPosition=0.00
TableTopLongitudinalPosition=-10.00
TableTopLateralPosition=0.00

[Beam0 - ControlPoint6]
CumulativeMetersetWeight=60.00
NominalBeamEnergy=0.010
NominalTubeCurrent=13
SpotSize=LARGE
GantryAngleIEC=0
GantryRotationDirection=NONE
TableTopVerticalPosition=0.00
TableTopLongitudinalPosition=-12.00
TableTopLateralPosition=0.00

[Beam0 - ControlPoint7]
CumulativeMetersetWeight=70.00
NominalBeamEnergy=0.010
NominalTubeCurrent=13
SpotSize=LARGE
GantryAngleIEC=0
GantryRotationDirection=NONE
TableTopVerticalPosition=0.00
TableTopLongitudinalPosition=-14.00
TableTopLateralPosition=0.00

[Beam0 - ControlPoint8]
CumulativeMetersetWeight=80.00
NominalBeamEnergy=0.010
NominalTubeCurrent=13
SpotSize=LARGE
GantryAngleIEC=0
GantryRotationDirection=NONE
TableTopVerticalPosition=0.00
TableTopLongitudinalPosition=-16.00
TableTopLateralPosition=0.00

[Beam0 - ControlPoint9]
CumulativeMetersetWeight=90.00
NominalBeamEnergy=0.010
NominalTubeCurrent=13
SpotSize=LARGE
GantryAngleIEC=0
GantryRotationDirection=NONE
TableTopVerticalPosition=0.00
TableTopLongitudinalPosition=-18.00
TableTopLateralPosition=0.00

[Beam0 - ControlPoint10]
CumulativeMetersetWeight=100.00
```

```
NominalBeamEnergy=0.010
NominalTubeCurrent=13
SpotSize=LARGE
GantryAngleIEC=0
GantryRotationDirection=NONE
TableTopVerticalPosition=0.00
TableTopLongitudinalPosition=-20.00
TableTopLateralPosition=0.00
```

# APPENDIX B – US NOISE FILTERING

The raw output signal from the US system, represented in blue in figure 51, presents some noise. The noise can be decreased by adding a capacitor to the US system. In this way the output of the US system without capacitor, with a 10 nF capacitor and a 100 nF capacitor were compared. Figure 51 shows a clear reduce of the US signal noise when a capacitor is added to the circuit. Looking to Table 5, the US system presenting the smallest mean standard deviation is the US system with a 10 nF capacitor, making it the one which will be used for the measurements requiring the US system.

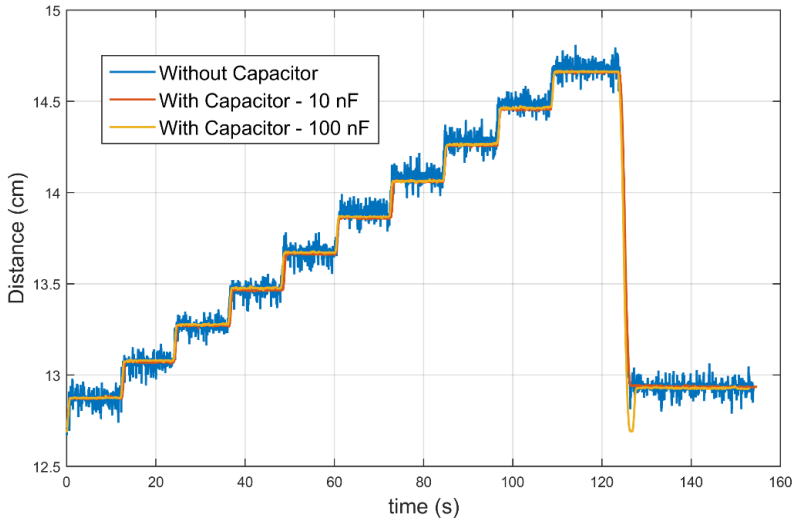


**Figure 51 –** Stage position data comparison for the longitudinal direction for 10 CPs acquired with the US system for 3 situations: US system without capacitor, US system with a 10 nF capacitor and US system with a 100 nF capacitor. The stage total distance was set to 2 cm during an irradiation period of 120 seconds.

**Table 5 –** Standard deviation calculated when the stage is stopped for 3 situations: US system without capacitor, US system with a 10 nF capacitor and US system with a 100 nF capacitor.

| **Standard deviation when the stage is stopped** | | |
|---|---|---|
| **Without Capacitor** | **With Capacitor** | |
| | **10 nF** | **100 nF** |
| 2.06E-02 | 3.10E-03 | 3.00E-03 |
| 2.31E-02 | 3.40E-03 | 3.50E-03 |
| 2.50E-02 | 3.50E-03 | 2.90E-03 |
| 2.13E-02 | 3.70E-03 | 4.50E-03 |
| 2.27E-02 | 2.90E-03 | 3.30E-03 |
| 2.25E-02 | 2.80E-03 | 3.30E-03 |
| 2.10E-02 | 2.50E-03 | 2.70E-03 |
| 2.02E-02 | 3.30E-03 | 2.40E-03 |
| 2.11E-02 | 2.40E-03 | 3.20E-03 |
| 2.24E-02 | 2.90E-03 | 3.40E-03 |
| **Mean of the standard deviation** | | |
| 2.20E-02 | 3.05E-03 | 3.22E-03 |

# APPENDIX C - NEED OF ADDITIONAL SPATIAL DEGREES OF FREEDOM IN SMALL ANIMAL RADIOTHERAPY

The gantry rotates in the y plane which corresponds to the axial plane. In Figure 52 a) y represents the vertical axis, x represents the lateral axis and z represents the longitudinal axis. The cranio-caudal direction corresponds to the z axis. The top of the gantry is located in the upper intersection of the 3 anatomical planes as represented in Figure 52 b) and the default gantry direction rotation is clockwise. Figure 52 c) represents the coronal plane and shows the initial reference position and the gantry direction default rotation which is clockwise.

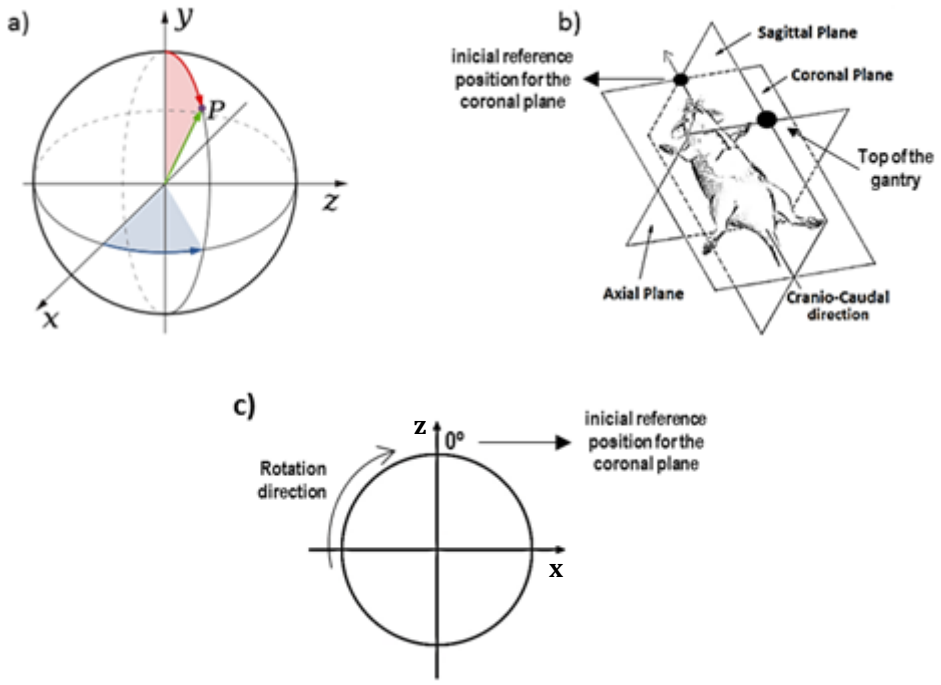


**Figure 52 –** a) Spherical coordinates. b) The three orthogonal anatomic planes of the rat body and reference points for the gantry with respect to the rat body orientation. c) Illustration of the initial reference position for the coronal plane and the gantry rotation direction considered in this thesis.

## C.1. Mouse glioblastoma case

**Table 6 –** Description of the beams used to simulate the different treatment cases for the mouse glioblastoma case.

| | Number of beams | Beam # | Type | Description |
|---|---|---|---|---|
| **Case 1** | 2 | 1 | Static | Beam delivered from the top of the gantry |
| | | 2 | Static | Beam delivered from the bottom of the gantry |
| **Case 2** | 1 | 1 | Dynamic | 360 degrees arc revolution |
| **Case 3** | 1 | 1 | Static | Beam rotated 60 degrees from the axial plane in the cranio-caudal direction |

## C.2. Mouse lung tumor case

**Table 7 –** Description of the beams used to simulate the different treatment cases for the mouse lung tumor case.

| | Number of beams | Beam # | Type | Description |
|---|---|---|---|---|
| **Case 1** | 2 | 1 | Static | Beam deviated 9 degrees from the vertical axis |
| | | 2 | Static | Beam deviated 261 degrees from the vertical axis |
| **Case 2** | 3 | 1 | Static | Beam rotated 30 degrees from the axial plane in the cranio-caudal direction |
| | | 2 | Static | Beam rotated 40 degrees from the axial plane in the cranio-caudal direction |
| | | 3 | Static | Beam rotated 50 degrees from the axial plane in the cranio-caudal direction |
| **Case 3** | 11 | 1 | Static | Beam delivered from the top of the gantry |
| | | 2 | Static | Beam deviated 9 degrees from the vertical axis |
| | | 3 | Static | Beam deviated 151 degrees from the vertical axis |
| | | 4 | Static | Beam deviated 353 degrees from the vertical axis |
| | | 5 | Static | Beam rotated 45 degrees from the axial plane in the cranio-caudal direction |
| | | 6 | Static | Beam rotated 55 degrees from the axial plane in the cranio-caudal direction |
| | | 7 | Static | Beam delivered in parallel with the corornal plane deviated 265 degrres from the inicial reference position for the coronal plane |
| | | 8 | Static | Beam delivered in parallel with the corornal plane deviated 270 degrres from the inicial reference position for the coronal plane |
| | | 9 | Static | Beam delivered in parallel with the corornal plane deviated 275 degrres from the inicial reference position for the coronal plane |
| | | 10 | Static | Beam delivered in parallel with the corornal plane deviated 285 degrres from the inicial reference position for the coronal plane |
| | | 11 | Static | Beam delivered in parallel with the corornal plane deviated 290 degrres from the inicial reference position for the coronal plane |

# APPENDIX D - TREATMENT BASED ON STAGE TRANSLATION

## D1. Mouse lung tumor case

**Table 8 –** Description of the beams for each stage position used to simulate the different treatment cases for the mouse lung tumor case.

| | Number of beams | Beam # | Type | Number of stage positions | Description |
|---|---|---|---|---|---|
| **Case 1** | 2 | 1 | Static | 1 | Beam delivered from the top of the gantry |
| | | 2 | Static | | Beam deviated 9 degrees from the vertical axis |
| **Case 2** | 1 | 1 | Dynamic | 316 | Beam delivered from the top of the gantry |

# APPENDIX E - SMALL ANIMAL PLATFORM PERFORMANCE BEFORE UPDATE

Initially the performance of the stage translation using protocols with different numbers of CPs was evaluated based on dose distributions. To assess the dose distributions, radiochromic EBT3 films were used. During the first experiments was discovered that the delivered dose was increasing with the number of CPs (Figure 53). To better understand this dose increasing with the increasing number of CPs, the US system was used to measure the stage translation distance and the irradiation period. The results are presented in Figure 54 and shows an increase of the irradiation period when the number of CPs increase. Once the error was found, an update was performed to the small animal platform and the error was fixed.

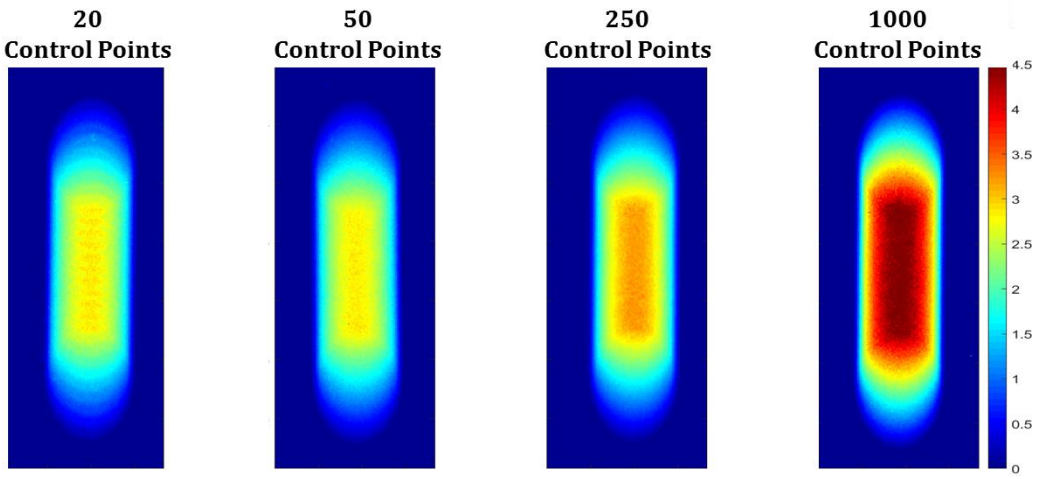


**Figure 53 -** Dose distribution measured with EBT3 films for 20, 50, 250 and 1000 CPs for a total longitudinal stage translation of 2 cm before the small animal platform update. A circular field with a diameter of 10 mm was used for collimation.

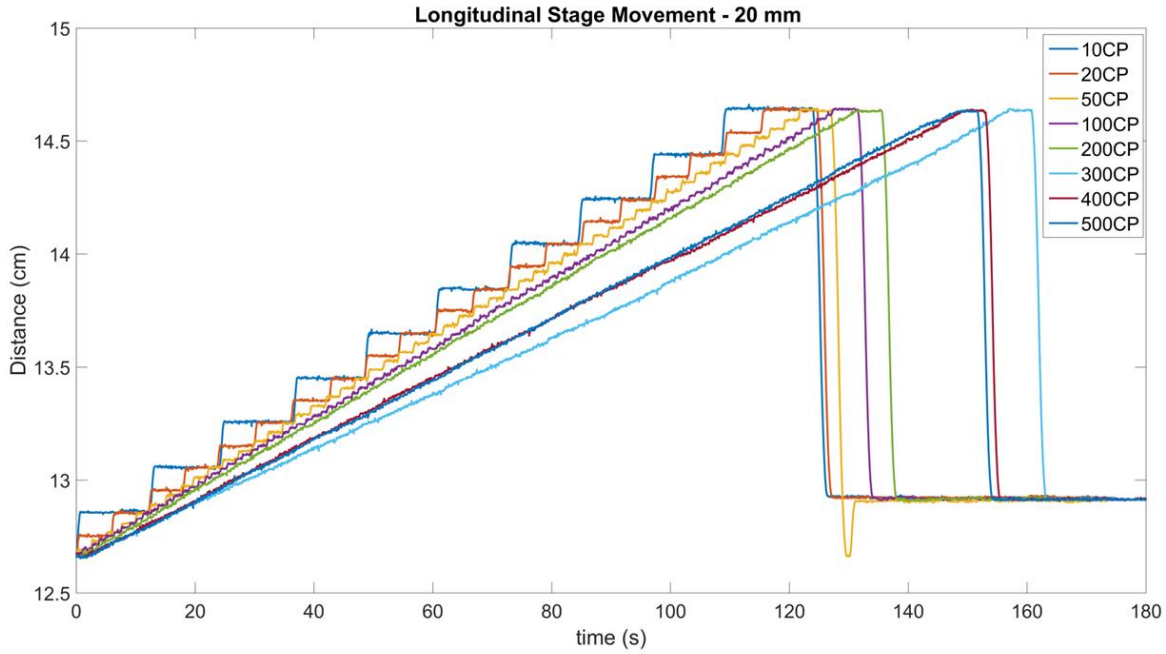


**Figure 54 -** Stage translation in the longitudinal direction for different numbers of CPs before the small animal platform update. The stage position was measured with the US system and the total distance was set to 2 cm.